APPROVAL SHEET

Title of Dissertation: Radar-based Non-contact Sensing for Smart Healthcare Applications

Name of Candidate: Elishiah J. Miller
Doctor of Philosophy, 2022

Dissertation and Abstract Approved: _____

Ting Zhu, Nilanjan Banerjee
Associate Professor, Professor
Department of Computer Science and Electrical Engineering

Date Approved: _____

ABSTRACT

Title of Document:	RADAR-BASED NON-CONTACT SENSING FOR SMART HEALTHCARE APPLICATIONS
	Elishiah J. Miller, Ph.D. Computer Science, 2022
Directed By:	Ting Zhu, Associate Professor; Nilanjan Banerjee, Professor; Department of Computer Science and Electrical Engineering

Today's healthcare system is seeing rapid technological advancements with the availability of vast amounts of information and computing resources. This has led to important developments in the field of smart healthcare for disease prevention and monitoring, diagnosis and treatment, hospital management, and health decision making. Smart healthcare utilizes technology such as internet of things (IoT) and enables physical sensing to collect information that can be processed and intelligently acted on to improve one's health. IoT devices have been used for monitoring physical health such as heartbeat, respiration, and sleep activities to name a few. Devices that must be worn for health monitoring can be uncomfortable and pose health concerns as they are potential carriers of bacteria and viruses. On the other hand, non-contact sensing is advantages by preventing the spread of bacteria and viruses as nothing is worn or touched. However, designing smart health systems that utilize non-contact sensing can be challenging due to environmental factors like noise, obstructions, and multiple people. Thus, in this dissertation we contribute to the field of smart

healthcare by showing how useful radar is for non-contact sensing. We showed how radar can preserve privacy, provide continuous monitoring, travel through material and obstructions, sense multiple people, and work well in challenging environments. These advantages are explored through three smart healthcare applications using radar-based non-contact sensing. Our applications use CW and FMCW radar for sensing and machine learning for thinking and driving intelligent decisions. We show how radar-based non-contact sensing systems can be deployed in the operating room for gesture control and at home to monitor coughing, sneezing, and medication tampering with high accuracy. Our three applications are built end-to-end and provide new ways for interaction and monitoring of health.

RADAR-BASED NON-CONTACT SENSING FOR SMART HEALTHCARE APPLICATIONS.

By

Elishiah J. Miller

Dissertation submitted to the Faculty of the Graduate School of the
University of Maryland, Baltimore County, in partial fulfillment
of the requirements for the degree of
Ph.D. in Computer Science
2022

Dedication

This dissertation is dedicated to my family. They have supported me emotionally, financially, and most important spiritually through the embodiment of Jesus Christ our lord and savior. To my wife who never let me quit and continuously reminded me that I can do all things through prayer with God. To my parents and sister who continued to encourage me and give me advice, support, and lots of cookies. Finally, to my father-in-law and mother-in-law who have helped care for my son and allow me to dedicate uninterrupted time to writing.

Acknowledgements

I would like to acknowledge the following people for their individual contributions to this dissertation and my graduate studies:

Dr. Ting Zhu and Dr. Nilanjan Banerjee for their continued support as my advisor and co-advisor. Dr. Ting pushed me to continue to write and publish three articles in the Smart Health journal. He continually reviewed my work and met with me countless times over skype. Dr. Banerjee helped me get into the PhD program at UMBC and guided me towards my research in using radars for non-contact sensing. I am deeply grateful for the opportunity to work with both professors.

I want to thank Dr. Helena Mentis who helped review my first work on non-contact sensing for gesture recognition in the operating room. Dr. Mentis gave me access to the simulation operating room at Arundel Mills Medical center where I was able to perform experiments and get feedback from real doctors.

I want to thank Dr. Kalpakis and Dr. Nirmalya Roy for serving on my PhD committee.

I want to thank all my supporters at the Johns Hopkins Applied Physics Laboratory (APL). Specifically, Dr. David Silberberg who served on my PhD committee and was also my group supervisor.

I would also like to thank Dr. Seth Martin and his team at Johns Hopkins Medicine for allowing me to collaborate with his research team and collect data at his research laboratory.

Table of Contents

List of Tables

List of Figures

Chapter 1: Introduction

Smart Healthcare

Today's healthcare system is seeing rapid technological advancements with the availability of vast amounts of information and computing resources. This has led to important developments in the field of smart healthcare for disease prevention and monitoring, diagnosis and treatment, hospital management, and health decision making. Smart healthcare can be viewed as a health service system that uses different kinds of technologies such as wearable and internet of things (IoT) devices to access health related information for making smarter decisions to improve people's lives (Tian et. al. 2019). As IoT devices and the like are pervasive and easily available, they can connect people, materials, and institutions related to healthcare faster than ever before. Additionally, IoT devices with cloud connectivity and embedded machine learning can actively manage and respond to medical ecosystems needs in an intelligent manner. Generally, smart healthcare solutions utilize technologies for sensing, thinking, and actions illustrated in Fig. 1. *1*. Sensing includes cameras, microphones, accelerometers, radars, and many others, which are used to collect physical information about one's health. Intelligent thinking is implemented with artificial intelligence through the development of machine learning and deep learning models. Actions can be taken with more available information leading to better healthcare.

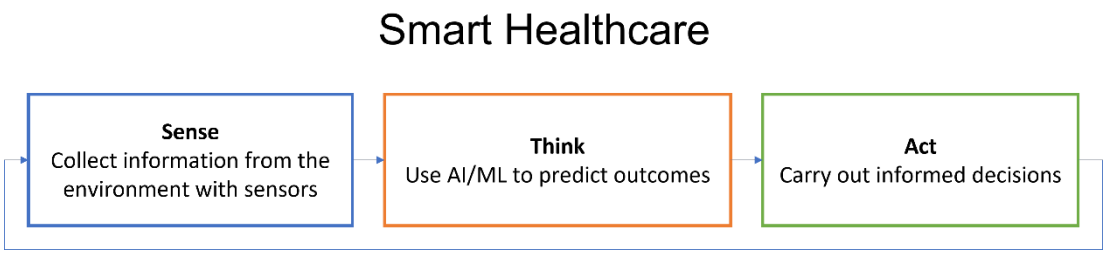

Fig. 1. 1. Smart healthcare process.

The process that enables smart healthcare to sense, think, and act has been realized through the development of smart healthcare applications such as obstructive sleep apnea diagnosis Tran (2019), non-contact sensing for Covid-19 Taylor (2020), and monitoring vital signs such as heartbeat and respiration Lv (2021). However, it can be challenging to design systems for complex and changing environments such as an operating room or a family home. Operating rooms have varying lighting conditions, dark and bright, tools, surgical methods, and requirements for sterility. Typically, wearables, camera systems, and headsets are used in an OR setting, but these systems are uncomfortable for people who wear or use them for long periods of time. In family homes there are obstructions such as walls, furniture, and interference can happen from multiple people in the same vicinity. Obstructions can cause systems that rely on light sensing to fail as they are blocked. Privacy is a concern as traditional sensing methods such as cameras and microphones collect personal identifiable data. Thus, there is a need for smart health applications that use non-traditional sensing methods such as radar. Radars have advantages of low transmission power, simple structure, high sensitivity, and can work in situations where light or audio-based sensing systems fail. Additionally, radars can preserve privacy and monitor health conditions in new and challenging environments. In this dissertation we explore three

smart healthcare applications using radar-based non-contact sensing to illustrate and address these concerns.

Dissertation Statement

A versatile design for smart healthcare applications utilizing radar for non-contact sensing is effective for building robust, unobtrusive, and privacy preserving systems that empower people to make informed decisions.

Radar-based non-contact sensing

Generally, radar systems built for smart healthcare are composed of four components which include: radar hardware, signal processing, gesture/activity/health monitoring and intelligent actions (Ahmed 2021). A basic radar hardware architecture will include transmitting and receiving antennas, a local oscillator used with a mixer to change the frequency of the signal, a band-pass filter, a power amplifier, and an analog to digital converter (ADC). Once a signal is transmitted and reflects off a human subject the received signal is demodulated to baseband, I phase I(t) and Q quadrature phase Q(t). Digital signal processing is then used to further process the quadrature I(t) and Q(t) signals. This typically involves amplifying the signal, reducing noise, converting the signal from analog to digital using an ADC, representing the signal in several formats, and using a Fast Fourier Transform (FFT) to detect objects at multiple distances. Depending on the application, the radar data can be expressed in time-amplitude for gesture profiling, range-amplitude for distance features, time-range for time varying distance features, and time frequency (Ahmed 2021). After selection of the signal representation, features can be created for training

machine learning algorithms for gesture, activity, and health recognition. The outcome from the machine learning models can then be used for intelligent actions to control and manipulate devices, monitor health, and send important health notifications.

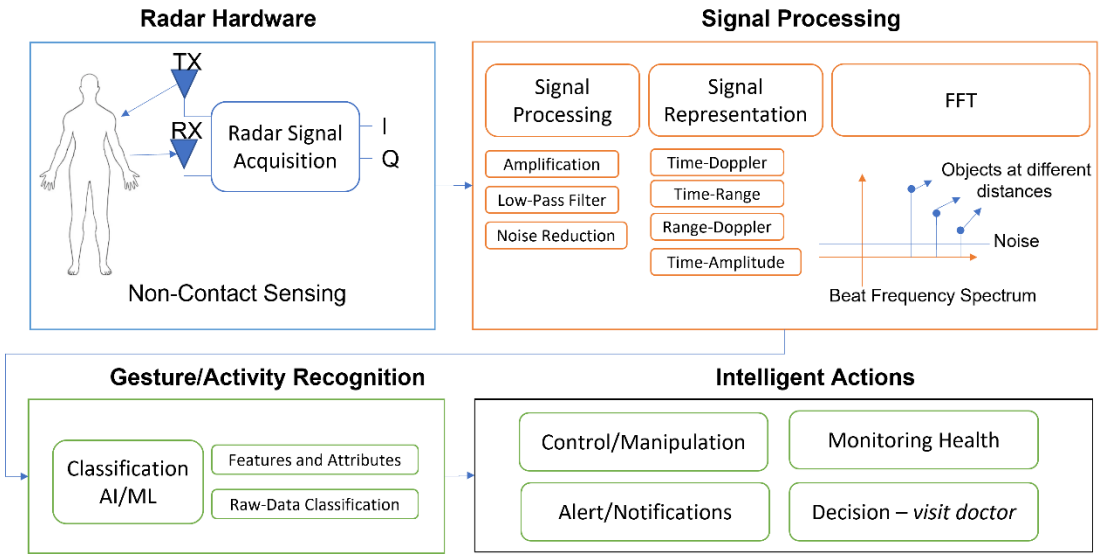

Fig. 1. 2. Radar-based non-contact sensing.

Radar-based non-contact sensing is achieved in this work using continuous wave (CW) and frequency modulated continuous wave (FMCW) radars illustrated in Fig. 1. *2*. CW radars utilize the Doppler frequency shift introduced by an object moving in the field of view (FoV) of the radar to detect the speed and direction or velocity of an object's motion. The advantages of CW radars are that they can be implemented on low-cost devices with simple front-end architectures and high sensitivity. Additionally, CW radars can have low analog to digital converter (ADC) requirements for sampling. Small sampling rates enable low power embedded digital signal processing. However, CW radars are limited as they are unable to detect distance to an object and typically sense a single moving object at one time. The CW radar does not modulate the frequency and has no time-of-flight (ToF) information

needed to calculate the distance from an object. When sensing multiple objects, the Doppler frequencies will overlap and make it difficult to distinguish one object from another.

FMCW radars extend CW radar architectures and can provide both Doppler and range information of objects. It is also possible for FMCW radar to detect multiple objects at the same time at different distances and distinguish objects with micro-Doppler and micro-range features. Sensing using FMCW radar begins with a synthesizer that generates a chirp signal and transmits the waveform out on a transmitting antenna. When an object moves in the FoV of the radar the waveform is reflected and obtained at the receiving antenna. Once the wave form is acquired the transmitted and received signals are mixed and down converted to the intermediate frequency (IF) signal. The IF signal is then processed most with an amplifier, then low-passed filtered and sampled with an ADC. The IF signal will have frequencies corresponding to reflections from multiple objects and can be observed by performing a fast Fourier transform (FFT) on each chirp signal. When processing the IF signal with the FFT, the frequency of the IF signal will be proportional to the range of the moving object. However, FMCW radars can consume more energy and require more complex architecture than CW radar. Additionally, the size profile of FMCW radars is larger and the displacement accuracy of an FMCW radar may not be as good as that of unmodulated CW system. The CW radar can easily achieve sub-millimeter accuracy in contrast to FMCW radar.

Given the limitations and advantages of CW and FMCW radar, we show how both CW and FMCW radar can be effectively used for smart health applications. We

show how CW radar can be used to create a small wearable device and detect simple hand gestures with low power. We then show how CW and FMCW radar can be used together to build systems for health monitoring for detecting coughs and sneezes with multiple people and for monitoring medication tampering in the home.

Dissertation Overview

In this dissertation we showcase the use of radar for non-contact sensing for three smart healthcare applications. The first smart healthcare application presented is a Doppler radar system for gesture control in the operating room enabling interaction while both hands are busy. The second smart healthcare application presented is a smart home monitoring system that uses a FMCW radar system for detecting cough, sneezing, and face touching. Finally, the third smart healthcare application presented is a monitoring system for medication tampering in the home. In summary the main contributions and scope of analysis can be defined as follows:

- A Doppler radar system for non-contact sensing and gesture interaction with medical images. Our system enables gesture control while both hands are busy with about 95% accuracy in an operating room setting.
- A smart home monitoring system that uses FMCW radar for detecting cough, sneezing and face touching with 96% accuracy. Our system can be deployed throughout a home for continuous monitoring and detection of activities through walls and with multiple people.
- An at home system using FMCW radar for monitoring medication tampering with 99% accuracy. Our system can classify eight tampering methods with three types of medication containers.

Chapter 2: Enabling one hand and no hands interaction for sterile manipulation of medical images using Doppler radar

Summary

In our first smart healthcare application we show how surgeons can interact with medical images using finger and hand gestures in two situations: one hand-free and no hands-free interaction. We explain how interaction with only one hand or a couple of fingers is beneficial and can help surgeons have continuous interaction, without the need to release their tools and leave the operating table, saving valuable patient time. To this end, we present RadSense, an end-to-end and unobtrusive system that uses Doppler radar-sensing to recognize hand and finger gestures when either one or both hands are busy. Our system permits the following important capabilities: (1) touch-less input for sterile interaction with connected health applications, (2) hand and finger gesture recognition when either one or both hands are busy holding tools, extending multitasking capabilities for health professionals, and (3) mobile and networked, allowing for custom wearable and non-wearable configurations. We evaluated our system in a simulated operating room to manipulate preoperative images using four gestures: circle, double tap, swipe, and finger click. We collected data from five subjects and trained a K-Nearest-Neighbor multi-class classifier using 15-fold cross validation, achieving a 94.5% precision for gesture classification. We conclude that our system performs with high accuracy and is useful in cases where only one hand or a few fingers are free to interact when the hands are busy.

Background

Healthcare professionals, such as surgeons, use imaging technology daily for providing patient care. One challenging use-case that surgeons face involves interacting with medical images in a sterile way, when either one or both hands are busy. The challenges are apparent as surgery is a collocated collaborate practice Mentis (2017) and the ability to learn and see the body is critical and difficult to achieve Mentis, Chellali, and Schwaitzberg (2014). To effectively communicate peculiar details of the anatomy, surgeons must talk, point, instrument tools, and interact with medical images while abiding by requirements for sterility Mentis (2017). When surgeons want to interact with images, they often hold tools in hand. To release or not release the tools is an important decision that the surgeon must make. In most cases, image interaction needs to occur while holding a surgical tool. In O'hara et al. (2014a, 2014b) they showed that there was a clinical need to provide image control while holding surgical instruments. For example, in minimally invasive procedures, where surgeons use small cuts and a camera to see inside the body, surgeons must hold a laparoscope and scissor tool while interacting with medical images Mondada (2003). How to control and interact with an imaging system while utilizing both hands is therefore critical and challenging. It was suggested in O'hara et al. (2014a, 2014b) that image manipulation, using gestures and voice commands, can be combined with the use of surgical tools, preventing the surgeon from removing gloves and re-scrubbing, which takes precious time. From this understanding, we explain how previous systems will not meet these requirements and how we

developed a new system that allows for finger and hand gestures in two situations: one hand-free and no hands-free interaction while holding surgical tools.

Previous gesture recognition systems, computer vision Mondada (2003); Tan, Chao, Zawaideh, Roberts, and Kinney (2013); Jacob, Wachs, and Packer (2013); Ebert, Hatch, Ampanozi, Thali, and Ross (2012); Feng et al. (2018); Ruppert, Reis, Amorim, de Moraes, and da Silva (2012) and wearable based Jalaliniya, Smith, Sousa, Büthe, and Pederson (2013); Schwarz, Bigdelou, and Navab (2011); Hettig et al. (2015), have been developed to help surgeons in fields such as radiology and urology interact with images in a sterile way. Many of these systems require the surgeon to release their tools and are uncomfortable and get in the way. For example, vision-based systems, Microsoft Kinect being the most popular, show that interaction with images requires the surgeon to use large hand motions to perform actions such as zooming in and out, panning, rotating, or changing the brightness. To perform these actions surgeons must stand at least four feet from the Microsoft Kinect, release their tools, and hold their hands positioned towards the device and monitor. In addition, tracking fingers while holding an object in hand is often a difficult task for the Kinect. Vision-based systems also require line-of-sight for interaction, are impacted by lighting, and fail when obscured by sterile drapes and sheets. On the other hand, wearable solutions do allow for interaction while hands are busy, but they are cumbersome and get in the way, as they most often use inertial measurement units (IMUs) or Electromyography (EMG) sensors, which require adherence to the skin, or the area being observed for gesture recognition.

To mitigate the disadvantages presented by computer vision and wearable devices, researchers Chi et al. (2018, 2016, pp. 1–10); Yao et al. (2018); Li and Zhu (2016); Khan et al. (2016); Li, Robucci, Banerjee, and Patel (2015) have proposed the use of ubiquitous ambient signals such as WiFi, Bluetooth, and radio frequency (RF) for robust gesture and activity recognition. Ambient signals allow for sensing in different environmental conditions without devices that have to be worn. Most of these systems have not been evaluated for gesture recognition with busy hands and utilize existing WiFi infrastructure, which we argue is problematic in a hospital setting. For example, devices connecting and reconnecting to the network limit network bandwidth, which affects system accuracy and response. The WiFi access points are typically omni-directional and pick up background motion, which adds noise to the system. Also, hospitals have multiple windows, floors, and rooms, which creates high risk for spotty WiFi dead zone connections with not enough coverage.

Dissertation Contributions

To this end, we developed a new hybrid, both wearable and non-wearable, gesture recognition system we call RadSense, short for radar sensing. RadSense is an end-to-end, mobile, and unobtrusive directional radar system, that uses the Doppler Effect to sense in-air hand and finger gestures for continuous sterile medical image interaction when one or both hands are busy. The system captures motion using radar and wirelessly transmits the motion via Bluetooth Low Energy (BLE) network to a computer for gesture classification and image control. The system can be worn on the human body or attached to an object with Velcro enabling unobtrusive gesture detection, as it is small and does not require adherence to the skin. Accurate gesture

detection can also occur when the system is covered by a sterile gown to meet requirements of sterility. We evaluated our system in a simulated operating room (OR) to manipulate preoperative images using four gestures: circle, double tap, swipe, and finger click shown in Fig. 1. *3*.

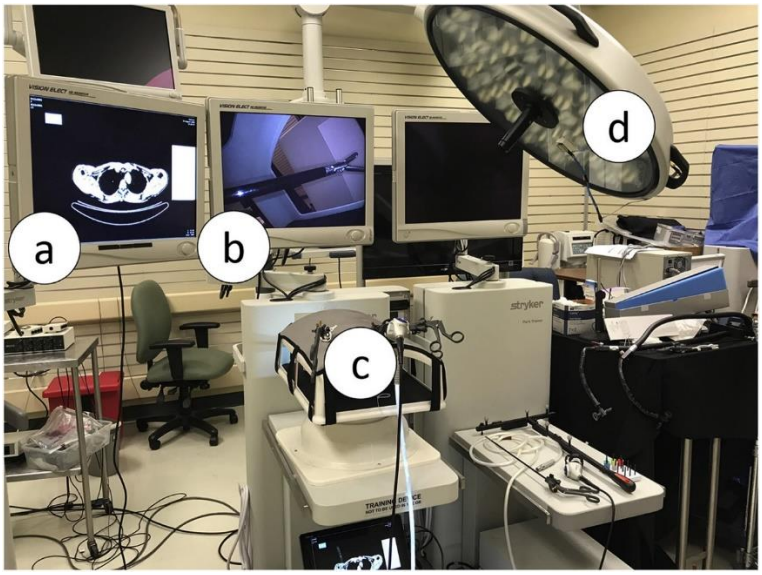

Fig. 1. 3. Simulated OR: the MicroDicom CT scan image viewer application (a), the laparoscopic view (b), the laparoscopic trainer (c), the radar attached to an overhead light (d).

We show how surgeons can use these gestures to interact with medical images in two situations: one hand free and no hands-free interaction. We collected data from five subjects and trained a K-Nearest-Neighbor multi-class classifier using 15-fold cross validation, achieving a 94.5% precision for gesture classification. The design, implementation, and evaluation of our system provides the following research contributions:

1. Design of a new end-to-end and unobtrusive gesture recognition system that uses radar and the Doppler effect for interacting with medical images. The

system can be worn and covered by a sterile gown or attached to an object for unobtrusive hand and finger gesture recognition while holding surgical tools.

2. Hand and finger gesture detection when either one or both hands are busy using only two features: zero-crossings and magnitude difference of the signal. We show that our system can detect gestures with a precision of 94.5% using a K-Nearest Neighbor classifier with low false positives.
3. An evaluation of our system in a simulated OR using four gestures: circle, double tap, swipe, and finger click.

Related Works

Touch-less gesture recognition systems help facilitate the sterile interaction between surgeons and the digital mediums they want to control de la Barre, Chojecki, Leiner, Muhlbach, and Ruschin (2009). In practice surgeons interact with two types of intraoperative imaging systems: a main display that shows the anatomy of the human body for operating, and a secondary display for pre-operative images Mentis (2017). For medical image interaction with these systems, several gesture recognition systems have been proposed and studied in literature with the focus in two main categories. This includes vision-based and wearable solutions. Each solution has its own set of limitations and advantages which we describe next.

Vision-based Approaches

Vast majority of research uses vision-based gesture recognition systems like the Kinect O'hara et al. (2014a, 2014b); Yusoff, Basori, and Mohamed (2013); Lopes et al. (2017); Gallo, Placitelli, and Ciampi (2011) to capture in-air arm, hand and

body motions, skeletal information, and voice commands for interacting with medical images. The Kinect uses depth, IR, color, and sound sensing. Fields such as radiology Tan et al. (2013); Jacob et al. (2013); Ebert et al. (2012, pp. 301–307); Feng et al. (2018) and urology Ruppert et al. (2012) have successfully used the Kinect to interact with 2D and 3D medical image data using hand and arm gestures. For example, Kenton O'hara et al. (2014a, 2014b) developed a gesture system for manipulating a 3D model in vascular surgery using the Kinect. In their study, they showed that surgeons could collaborate, communicate, and interact with the system in a sterile way using one hand, two hands, and voice controls. The surgeon, however, is unable to hold a tool and track a finger, as the Kinect is more suited for hand, arm, and body tracking. For more fine-grained gestures, research has turned to devices for finger tracking like the Leap motion Bizzotto et al. (2014, pp. 655–656); Cho, Lee, Park, Ko, and Kim (2018). The Leap Motion can accurately track objects while being held in the hand. A touch-free medical interface, using Leap motion, was developed in Nathaniel Rossol (2014), tracking a pen while being held in the hand for gesture recognition. When compared to the Kinect, Leap motion has a smaller field of view (FOV) and shorter-range detection. We argue that positioning the device near the FOV of the surgeon’s hands, while operating can therefore be difficult. It was shown in P. Hughes (2015) that surgeons prefer the Kinect over the Leap motion due to its wider FOV and range, but found the Kinect to be tiresome, as surgeons were physically exhausted from holding their hands and arms up. Although useful, vision-based systems are limited by their range of detection, require line-of-sight sensing for interaction, are affected by lighting conditions [14], and fail when obscured by sterile

drapes and sheets. Unlike vision-based approaches, our system is instrumented with a radar, capable of detecting hand and fine-grained finger motion while holding surgical tools. Our system is not as sensitive to lighting conditions and can travel through material, with the ability to be placed behind a sterile gown or attached to an overhead medical light for interaction.

Wearable Approaches

Devices that can be worn on the human body, often requiring attachment to the skin and body parts, known as wearables, have been used for gesture interaction with medical images. For example, Shahram Jalaliniya et al. Jalaliniya et al. (2013) used inertial measurement units (IMUs) worn on the wrist and pressure sensitive floors (non-wearable) for detecting hand and foot gestures to interact with medical images. In addition, the use of inertial sensors Schwarz et al. (2011, pp. 129–136) worn on the body have been used for multiple user-defined gestures by tracking relative pose within a performed gesture. While others have used commercial products like the Myo arm band Hettig et al. (2015) for exploring 3D medical image data. We argue that these systems are uncomfortable, having to touch the skin, and are obtrusive, getting in the way of surgeon, not allowing the use of gestures while holding surgical tools. Our radar gesture interface can also be worn, but does not require attachment to the arm, hands, or skin of the surgeon. Instead, our radar can be attached on the chest via Velcro. We argue that this allows for an unobtrusive way to recognize gestures that may be more comfortable. Furthermore, we can attach our radar to other objects, such as a overhead medical light, for gesture interaction. In both cases, our system can be used while holding surgical tools.

System Design

The RadSense system (see Fig. 1. *4*) allows a surgeon to perform gestures, while holding surgical tools, to interact with secondary intraoperative imaging systems. The system allows the surgeon to remain at the operating table, not having to release tools or scrub out to interact with images. The system works by using directional radar, to minimize background noise, and the Doppler effect to capture hand and finger motion. This motion is captured from the radar using a custom-built data collection module. The data collection module sends the captured motion to a data relay unit which transmits the motion to a computer via BLE. The computer then receives the motion detects and classifies gestures, which are then used as commands to control a secondary intraoperative imaging system. In the following sections we describe the details of how to interact with our system through gestures, how our system captures hand and finger motion for gesture detection, the hardware components of the system, an algorithm we developed to detect gestures with high precision, and the features we use to reliably distinguish gestures for classification.

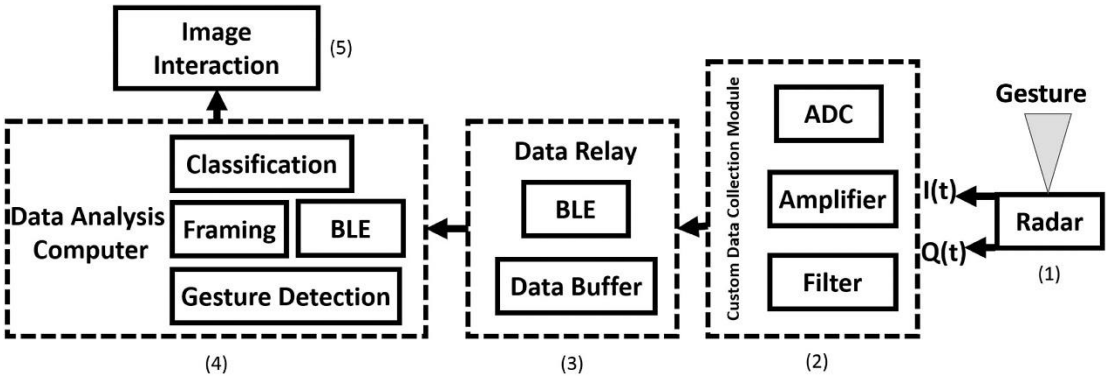

Fig. 1. 4. System architecture design: from right to left, radar (1), custom data collection module (2), data relay (3), data analysis computer (4), image interaction (5).

Doppler Effect and Quadrature Signal Processing

Our system uses the well-known Doppler effect or Doppler Shift principal to sense hand and finger motion. The Doppler Shift phenomenon is observed when a source emits a signal that is reflected by a moving object and the received signal is observed to have a change in frequency. In our approach, we chose a radar that has the source and receiver co-located. When a user moves their hand or fingers toward or away from the radar, it reflects the emitted radio waves causing a shift in frequency. The received signal captured by the radar can be described by the following equation:

$$f_r = f_t(\frac{c+v}{c-v})$$

where, f_r is the frequency of the received wave, f_t is the frequency of the transmitted wave, v is the velocity of the object (moving hand/fingers), and c is the speed of light. The shift in frequency is defined as $f_d = f_r - f_t$ and can be used to determine gestures.

Detecting the Doppler shift from hand and finger motion is done using quadrature signal processing. First, our radar system demodulates from equation (1) into the baseband in-phase I and quadrature-phase Q. Demodulation is a process of detecting a received signal represented as a quadrature signal with real part I and complex part Q. In radar applications we can represent quadrature signals as complex numbers with in-phase I referring to the momentary amplitude of the real-signal and the quadrature-phase Q referring to the momentary amplitude of the real signal shifted by 90°. Once we obtain the demodulated I and Q components we can calculate the phase of the signal to determine direction of the hands and fingers. To do this we

use the differentiated and cross-multiply algorithm (DACM) proposed in Wang et al. (2014) to compute the instantaneous phase of the quadrature signal to obtain from equation (1). A positive phase value describes an object moving toward the radar and a negative phase value describes an object moving away from the radar. We use this principle to detect the direction of the hands and fingers moving towards and away from the radar. The DACM algorithm given in discrete form Wang et al. (2014), i.e.:

$$\Theta(n) = \sum_{k=2}^{n} \frac{I(k) * [Q(k) - Q(k-1)] - Q(k) * [I(k) - I(k-1)]}{I(k)^2 + Q(k)^2}$$

where theta Θ(n) represents the instantaneous phase and $I(k)$ and $\boldsymbol{Q}(k)$ represent the $\boldsymbol{k^{th}}$**,** I and Q channel sample from the frame of size n. We chose the DACM algorithm as it has advantages over the widely used arctangent demodulation method that can handle the phase discontinuity problem by automatically phase unwrapping for phase reconstruction without ambiguities Gu (2016).

Gesture Set and Interaction

We created four initial gestures that can be used for interaction with the secondary intraoperative imaging system shown in Fig. 1. *5*(a–d). Our system is not restricted to this gesture set as any gesture can be created by following a set of rules. The rules include varying the length of a gesture, making one motion longer than the other, varying the size of the gesture, making a large motion with the hand compared to a small gesture with the finger, and the location of the gesture, far or close to the radar sensor. We used these rules to develop four initial gestures that can be used while holding surgical tools in two cases described next.

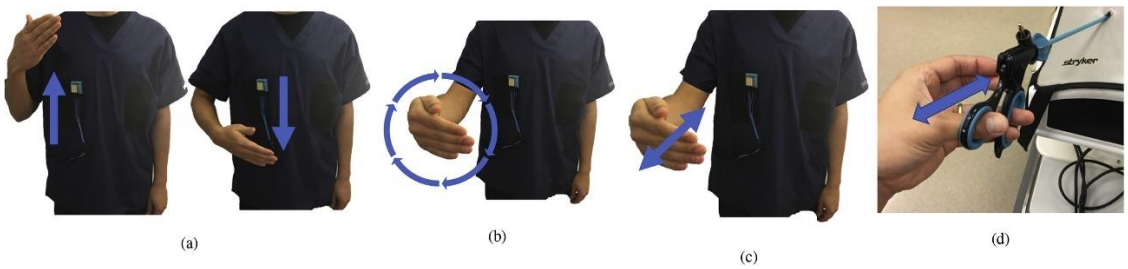

Fig. 1. 5. Gesture Set: swipe (a), circle 5 (b), double tap (c), and finger click (d).

One Hand-free Interaction

One hand interaction involves the surgeon having only one hand free to perform hand gestures and interact with images. In this scenario the surgeon can hold a surgical tool in one hand while still performing gestures with the second hand, shown in Fig. 1. *6*. The radar is worn on the chest of the surgeon for gesture detection. In this position, the surgeon can perform the following three gestures while holding one tool: hand swipe to scroll through images, a hand circle switch between commands, and a hand double tap to flip an image left or right (see Fig. 1. *5*(a–c)). The hand swipe occurs in front of the chest, the arm extended half the length of the arm, with a swinging motion either up or down. The circle is performed with the arm extended in front of the chest, the hand then moves either clockwise or counterclockwise, and performed five times, named circle 5 gesture, in order to create a long distinguishable gesture. The double tap occurs with the arm extended as far as possible in front of the chest. The four fingers of the hand are then moved towards the palm and then away from the palm twice.

Fig. 1. 6. One hand interaction: viewing the image (a), performing a gesture (b), RadSense worn on chest (c) busy hand holding tool (d).

No Hands-free Interaction

No hands-free interaction involves the surgeon having no hands free, but only the index finger available to perform gestures. In this scenario the surgeon can hold two surgical tools, one in each hand while still being able to interact with medical images, shown in Fig. 1. *7*. For example, if using a laparoscopic grasper or scissors, the index finger used to manipulate the end effector is free. For this configuration, the radar is attached to an overhead medical light, to be in view of the finger. In this position, the surgeon can perform a finger click gesture, like pulling a trigger and then releasing, to flip an image left or right. Performing the same click can also be used to toggle between flipping left or right. In this case the radar is attached to an overhead medical light, angled towards the finger for gesture detection.

Fig. 1. 7. No hands interaction: RadSense attached to medical light (a), viewing image (b), performing finger gesture while holding a tool (c) busy hand holding tool (d).

Hardware Design

The hardware for our system (see Fig. 1. *8*) uses the K-LC2 25-GHz K-band Doppler radar transceiver RFBeam (2016), a custom-built data collection module, and a RFduino micro-controller to obtain the demodulated I and Q signal channels for gesture recognition. Our hardware design is simple, small, and low cost; all components total less than $80. In the following sections, we introduce the major subsystems of our hardware platform.

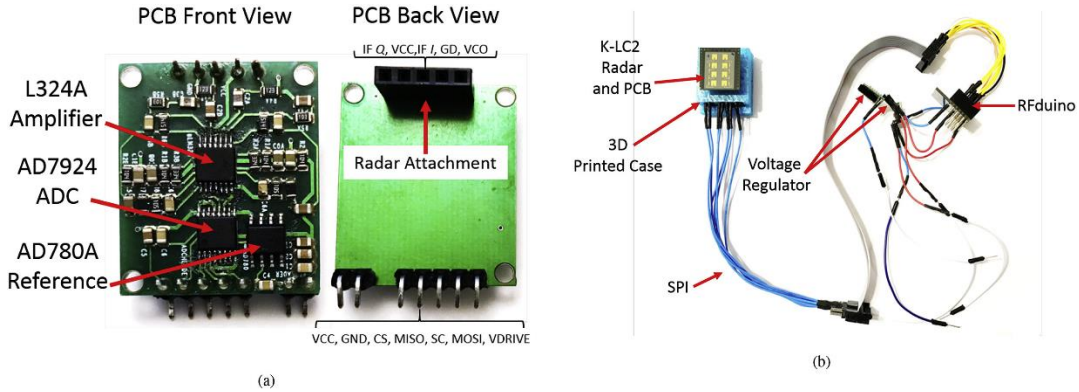

Fig. 1. 8. Custom PCB design (a), including the front view of the circuitry (left), and back view of the radar attachment (right), and the Wearable Radar Interface design (b).

To sense hand and finger motion, we used the K-LC2 continuous wave (CW) radar, capable of sending Doppler shifts. The K-LC2 cannot be used to detect the range or distance of an object, but only displacement of movement of the object due to lack of modulated spectral information Gu (2016). Two other types of radar technology exist known as frequency modulated continuous wave (FMCW) radar and pulse or impulse radar. These two types of radar are capable of sensing range information. We chose CW radar over FMCW and impulse radar as CW radar has higher accuracy in detecting movement, can operate in low power, and requires simpler hardware and signal processing techniques to condition the input signal Gu (2016).

To capture hand and finger motion, we designed a custom data collection module which connects to our radar, by leveraging the design in Li et al. (2015). To do this we created a printed circuit board (PCB), that amplifies and applies a low-pass filter on the captured I and Q signals, from the radar, for short-range movement detection. We define short range as the distance from the chest of a subject to end of their arm fully extended. The data collection module includes a 12-bit ADC that is used to transmit the I and Q signals to a Simblee RFduino micro-controller via a serial peripheral interface bus (SPI). We housed the data collection module inside a 3D printed case with Velcro attached to the back side. The Velcro allows our system to be worn on the human chest or attached to an object such as an overhead medical light for gesture detection.

To transmit the hand and finger motion from our custom data collection module to a computer, we designed a data relay module. Our data relay module uses the Simblee RFduino micro-controller. This micro-controller houses an ARM Cortex-M0, running at 16 MHz, and a BLE module used to transmit the digital I and Q signals sampled every 3 milliseconds to a central computer.

The radar module consumes 35 mA at 5 V (0.175 W), the RFduino consumes 10 mA at 3.3 V (0.033 W), L324 consumes 0.8 mA at 3 V (0.0024 W), the AD7924 consumes 2 mA at 3.0 V (0.006 W), and the AD780 consumes 1 mA at 3.0 V (0.003 W). The total power consumption of the wearable radar interface is 0.2194 W while transmitting data. A 3.7 V lithium-ion rechargeable battery is used to power our system with appropriate step up/down regulators. The RFduino micro-controller program uses less than 24KB of memory.

Gesture Detection

To reliably classify gestures, we developed a highly precise real-time gesture detection algorithm shown in Fig. 1. *9*. Our detection algorithm is used to detect the start and end of a gesture. Once the start and end of a gesture has been determined we calculate a set of features to classify gestures. We also create a simple threshold to determine if there is no movement explained next.

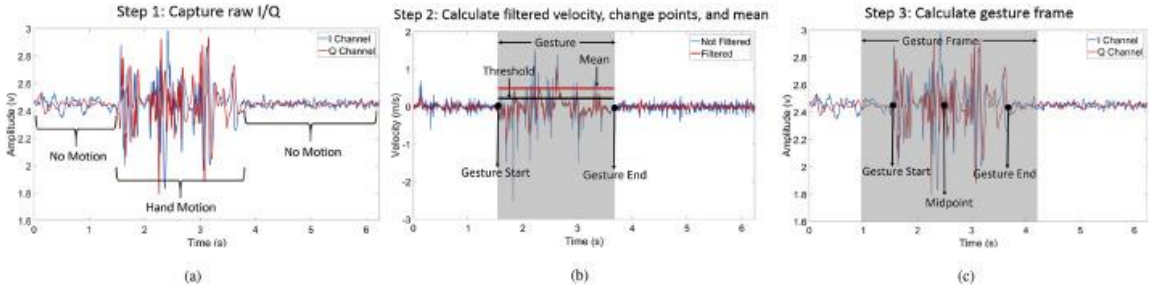

Fig. 1. 9. Gesture detection algorithm: step 1, capture the raw I and Q with 2080 samples (a), step 2, calculate the velocity of motion, filter the velocity with Savitzky-Golay filter, calculate the change points that indicate the start and end of the gesture, and compare the gesture mean with a predetermined threshold (b). If the mean is greater than the threshold, we continue to step 3 and calculate the I/Q gesture frame by finding the midpoint between change points and extending the frame 520 samples to the left and right (c).

In step 1, we capture a frame size of 2080 samples of raw I and Q channel values from the radar shown in Fig. 1. *9* (a). We chose a frame size of 2080 by observing the average window size used during labeling for data collection which was about 1040 samples. We wanted a larger frame size, double in our case, to allow for our frame to include additional motion information for easier detection as our gestures create an impulse in the signal and then flat lines. This window size corresponds to about 6.23 s of motion for 2080 samples, sampled every 3 milliseconds.

In step 2, We find the start and end points within the captured frame shown in Fig. 1. *9* (b). To do this we calculate the velocity of the I and Q quadrature signal by taking the forward difference of the instantaneous phase using the DACM algorithm shown in equation (2). The forward difference is then calculated as:

$$\Theta_d(n) = \Theta(n+1) - \Theta(n)$$

where $\Theta_d(n)$ represents the phase difference corresponding to the gesture velocity. To de-noise the velocity signal while maintaining the shape of its original curve we apply a Savitzky-Golay (SG) filter with polynomial order equal to 21 and frame length equal to 89. The filtered velocity signal is a good indicator for detecting hand and finger motion as little motion happens between +0.2 m/s and −0.2 m/s and hand and finger motion happens outside this range. In Fig. 1. *9* (b) there is a larger

variation in velocity where the gesture happens compared to where there is no movement. We use this observation to calculate the change points by observing where the root-mean-square (RMS) level of the velocity signal changes most significantly. The inflexion points help us identify the start and end of a gesture. For our purposes we want to identify two inflexion points that divide our gesture frame into three sections. We use the changepoint detection method Lavielle (2005); Killick, Fearnhead, and Eckley (2012) to find two change points $K = 2$, by minimizing the function:

$$J(K) = \sum_{r=0}^{K-1} \sum_{i=K_r}^{K_{r+1}-1} \Delta(x_i; \chi([x_{K_r} \ldots x_{k_r+1} - 1])) + \beta K$$

where $J(K)$ is the total residual error from the three sections for two change points $K = 2$, for a given signal $x_{k_r}, \ldots, x_{k_{r+1}} - 1$, given the empirical estimate χ and the deviation measurement Δ, where β represents the fixed penalty added for each change point. We use the RMS empirical estimate statistic and find two change points indicating the start and end of a gesture. After finding the two change points we calculate the mean of the velocity signal between the two change points. We created a threshold +0.2 m/s by averaging a total of 60 s worth of collected velocity values with no movement. If the mean of the velocity signal, defined by the change points, falls below this threshold we ignore the gesture and consider it as no movement. In the other case we continue to step 3.

In Step 3, we calculate the midpoint between the two change points and extend our frame 520 samples to the right and to the left of the midpoint Fig. 1. *9* (c).

We use these left and right points for the start and end of our raw I and Q channel gesture frame. If the gesture is off center within the 2080 sample frame and we cannot extend our frame to the right or to the left by 512 samples, we truncate the frame to the max sample less than 512. At this point our gesture is still unknown, but we are more confident that a gesture happened. Our gesture frame is now created, and we can continue to calculate features to classify the gesture.

Feature Extraction

We experimentally developed two features to reliably classify our four gestures. To do this we extract two features from our captured gesture frame of 1040 samples. Previous works have used zero-crossing Gao et al. (2016) and the magnitude differences between the highest crest and the lowest crest through each signal Wan, Li, Li, and Pal (2014) achieving above 90% accuracy for classification. Also, the set of measurable properties using the Doppler effect were described in Gupta, Morris, Patel, and Tan (2012) for sound waves that are also applicable to radar. We base our feature set off this work and show how we can obtain higher than 94% accuracy for classification explained in our evaluation section. The two features are described next.

The first feature we calculated was the sum of the zero-crossings of the quadrature signal. We normalize each channel so that the signal is centered at zero along the x-axis. The zero-crossings is proportional to the phase of the signal. To find the zero crossings for each channel, I and Q, we look for the following conditions: $X_i < 0$ and $X_i - 1 > 0$ and $X_i > 0$ and $X_i - 1 < 0$ where X_i represents the i^{th}

sample for channel I or Q. We then take the sum of all zero-crossings found for both I and Q as a feature.

The second feature we calculate is the difference of the maximum, minus the minimum, magnitude. The magnitude of the signal is proportional to the amplitude of the signal. The amplitude is higher when the hand and fingers approach the radar and lower when they recede. The magnitude difference is calculated as:

$$\hat{M} = max(M(t)) - min(M(t))$$

where $\hat{M}$ is the magnitude difference, and $M(t)$ is the magnitude defined as:

$$M(t) = \sqrt{I(t)^2 + Q(t)^2}$$

where t is the t^{th} sample of the signal.

When the two features, discussed previously, are used together, they cluster the feature set into 4 categories (see Fig. 1. *10* (a)). This is important as it makes our machine learning model more accurate. The magnitude difference helps distinguish a large gesture, hand performing circle 5 gesture, from a small gesture, finger performing finger click. The sum of the zero-crossings help distinguishes between the length of the gesture, short, finger click and double tap, or longer, swipe and circle 5. The two features we chose may make our system less robust if additional gestures are added. To retain the high accuracy of our system, we suggest to use additional sensors, each with their own trained models of just a few gestures. Thus, the gesture set can be extended by adding more sensors.

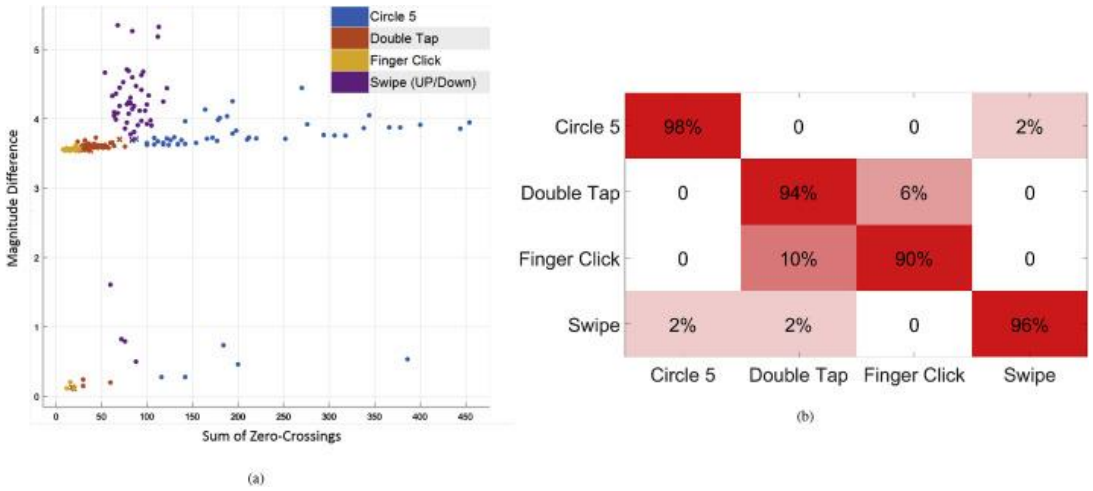

Fig. 1. 10. Sum of zero crossing features, and magnitude difference, the circle indicates correct prediction and x indicates incorrect prediction (a), and Confusion matrix classification accuracy for radar training data (b)

Evaluation and Results

We evaluated our system in a simulated OR, by training a K-Nearest-Neighbor (KNN) multi-class classifier using a 200 labeled gesture data set composed of the sum of the zero-crossings and magnitude difference features described previously. We collected our data from five subjects, with Institutional Review Board (IRB) approval, two male, and three female. Each subject was asked to perform our four gestures 10 times each. We trained each subject on how to perform gestures, and then collected the gesture data. We used a camera to record video of the gestures for accurate labeling of each gesture. The magnitude difference (y-axis) and sum of zero-crossings (x-axis) features are shown in Fig. 1. *10* (a).

For the KNN model we used the Euclidean distance and squared inverse distance weight with K = 10 for the number of nearest neighbors. We evaluated our trained KNN model using 15-fold cross validation achieving 94.5% accuracy

calculated from the confusion matrix (see Fig. 1. *10* (b)). In detail we take the 200 examples divide them into 15 equal folds (13 examples per fold), then randomly shuffle the folds. Then K-1 folds are used for training (15-1 = 14) and the last fold (1) is used for validation. This process is repeated K (15) times, leaving one different fold for validation each time. After each K-iteration we calculate the classification accuracy and then take the average of all iterations for mean classification accuracy (see Fig. 1. *11* (a)). In addition, we varied the number of folds and found 15-fold cross validation to have the highest accuracy (see Fig. 1. *11* (b)). For comparison, we also trained three additional models using 15-fold cross validation: cubic support vector machine (SVM) achieving 94.5% accuracy, Ensemble Bagged Trees (EBT) achieving 91% accuracy, and Fine Decision Tree (FDT) achieving 90% accuracy (see Fig. 1. *12*). In addition, we varied the number of folds for cross validation for the KNN: 5-fold achieving 93% accuracy and 10-fold achieving 93.4% accuracy. We also varied the features and found that using both features resulted in the highest accuracy of 94.5%.

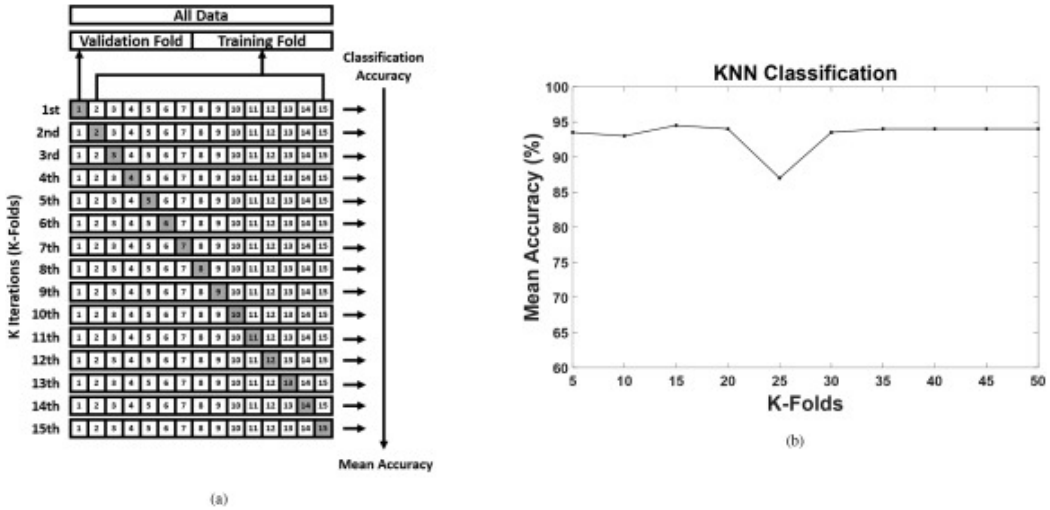

Fig. 1. 11. K-Fold cross validation process (a), and Evaluation of K-Fold cross validation (b)

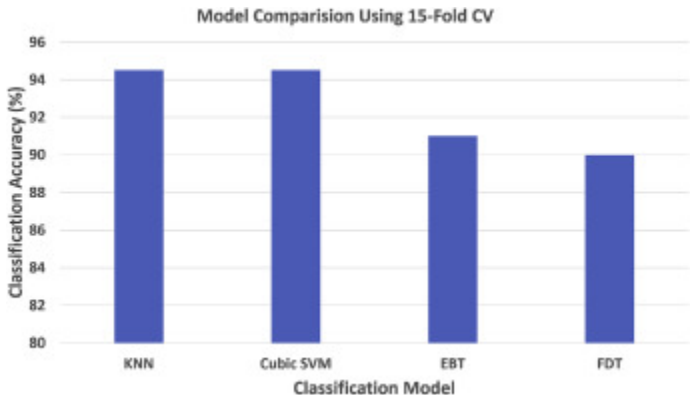

Fig. 1. 12. Model comparison using 15-fold cross validation.

System Precision and Recall

To evaluate our trained KNN model we analyzed the precision and recall of our confusion matrix Table 1. *1*. Precision measures the proportion of positive identifications of gestures that were correct. Recall measures the proportion of actual positive gestures that were correctly identified. We can see in Table 1. *1* that the precision for circle 5 is 0.98, with 2% classified as swipe, with recall 0.98. The precision and recall for double tap is 0.94 with recall of 0.8668 with 6% classified as finger click. The precision and recall for finger click is 0.90 with recall 0.9375 with 10% being classified as double tap. The swipe gesture precision is 0.96 and recall is 0.9796, with 2% of the gestures classified as circle 5 and another 2% classified as double tap. The biggest discrepancies were between the double tap and finger click gestures as they were similar in movement (two motions) and distance (arm length similar to distance between overhead light and finger position).

Table 1. 1 System training precision and recall

Gesture	Circle 5	Double Tap	Finger Click	Swipe
Precision	0.9800	0.9400	0.9000	0.9600
Recall	0.9800	0.8668	0.9375	0.9796

Detection Through Material

We also found that our system can reliably classify gestures when covered by material (see Fig. 1. *13* (a)). This is particularly useful for meeting requirements of sterility, as surgeons can wear the RadSense system underneath their sterile gown. We performed a preliminary evaluation and trained a new, supervised KNN model and removed the finger click gesture. In this experiment, we had one subject wear the radar on the left side of the chest and then wear a sterile gown over the radar. The subject performed each gesture 10 times each. We were able to achieve an accuracy of 97% when covered by a sterile gown (see Fig. 1. *13* (b)). The precision and recall are shown in Table 1. *2*.

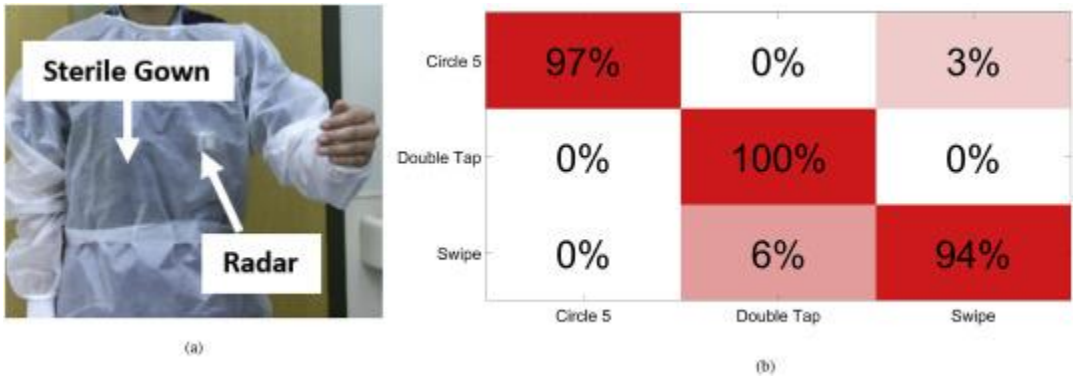

Fig. 1. 13. The radar worn on the chest of a subject behind a sterile gown (a), and the confusion matrix results when the radar is covered by the sterile gown (b).

Table 1. 2. Training precision and recall for through material detection

Gesture	Circle 5	Double Tap	Swipe
Precision	0.9700	1	0.9400
Recall	0.9691	1	0.9434

Discussion

We tested our system in a simulated OR (see Fig. 1. *3*). We used a monitor to display CT scan images using the MicroDicom application. Images were retrieved from the national institute of health (NIH) national biomedical imaging archive

(NBIA). The MicroDicom application allows for scrolling, zooming, rotating, panning, measuring, and drawing on a CT scan image. Finally, we mapped our gesture set to a set of commands to control the CT scan images. We mapped the following gestures to the following commands: swipe to scrolling up and down, double tap to flip the image left and right with the hand, finger click to flip the image left and right, done while holding a surgical tool, and circle 5 to switch between commands, up or down for swipe, and left or right for double tap and finger click.

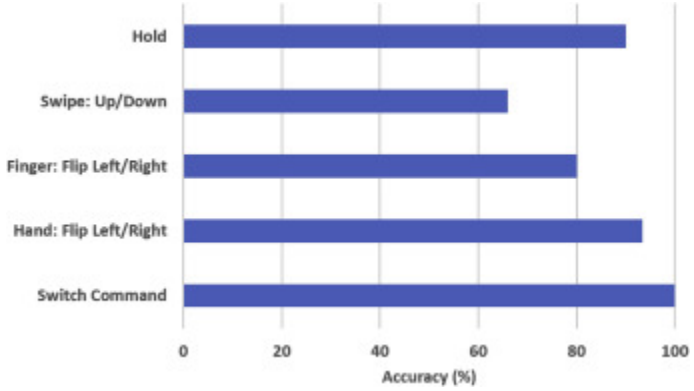

Fig. 1. 14. Accuracy of commands when using real-time system

We tested our commands by having five subjects perform the gestures 10 times each then took the average of correctly executed commands. The system was able to detect gestures and control the CT scan images shown in Fig. 1. *14*, but future work is required to analyze the usability and failure rate of our system. The real-time system was particularly bad at detecting the swipe gestures as we observed that users swiped too close to the radar or shifted the radar up and down on the shirt when performing a swipe. Also, the finger click gesture, often was classified as a double tap, but since they were mapped to the same command users did not notice. This miss-classification between the finger click and double tap was not a big issue for users, as the two gestures were used in two different configurations: one hand

interaction (using the hand) or no hands interaction (using the finger). The hold gesture was not explicitly trained, but rather, any movement below our threshold was assumed to be a hold.

Chapter 3: Smart homes that detect sneeze, cough, and face touching

Summary

In our second smart healthcare application we developed a wireless sensing system capable of detecting voluntary coughs, sneezes, and face touching with alert based notifications sent to a mobile application. Our work is motivated by the fact that coughing, sneezing, and face touching activities are three primary ways of spreading disease. With the onset of COVID-19 it is paramount to monitor these activities at home and practice good hygiene. To do so, our system uses radio frequency technology to capture motion, speed, direction, and range information from human activities. It does this by using a combination of a continuous wave Doppler and frequency modulated continuous wave radar. By observing a set of features related to the sensed motion, we designed a set of fuzzy logic IF-THEN rules that can differentiate each activity from each other with an overall accuracy of 96%. In addition, our system enables smart homes to detect and localize these activities at different distances up to 2.74 m, through walls, and with multiple people. We envision our system helping not only with prevention of COVID-19 but supporting contact tracing efforts by monitoring people's activities at home.

Background

The rampant and rapid spread of COVID-19 is unrelenting and its impact on healthcare has been devastating. As the writing of this paper, there has been a total of 11, 590, 195 confirmed cases and 537,429 deaths globally with the United States leading with 2,935,008 confirmed cases and 130,284 deaths according to the Johns

Hopkins University (JHU) (JHU 2020). To combat this pandemic, several guidelines have been issued by the Centers for Disease Control and Prevention (CDC) (CDC 2020) and the World Health Organization (WHO) (WHO 2020). The guidelines suggest that people wash their hands often, avoid close contact, cover their mouth and nose with a face cover, avoid touching their face, cover coughs and sneezes, clean and disinfect often, and monitor health daily. In addition, contacts with people testing positive for COVID-19 are asked to stay home and maintain a social distance of six feet from others for at least fourteen days. Thus, there is a need for at home monitoring systems to track and locate people's activities to help people properly clean and maintain proper hygiene and social distancing.

Dissertation Contributions

This has motivated us to research a new smart home monitoring system shown in Fig. 1. *15*, that alerts people of activities related to coughing, sneezing, face touching, and entering and leaving a room. In contrast to previous works which have mainly used audio sensing Birring et al. (2008); Sun et al. (2011a, pp. 425–434) or wearable and portable sensors Drugman et al. (2019); Jasmine and Jayanthy (2020), our system uses radio frequency (RF) technology to capture the motion characteristics of activities performed by humans. Previous systems are limited and suffer from environmental sounds and obstructions, are often required to be worn, making them obtrusive and uncomfortable, have dependence on batteries reducing monitoring time, and have privacy concerns because of microphone recordings. We address these issues by using a combined continuous wave (CW) and frequency modulated continuous wave (FMCW) radar that can detect motion, speed, direction, and range

information from human activities. Our system is unobtrusive, as it can be mounted to a wall or stand in a room and can continuously monitor activities with an overall accuracy of 96%. In addition, our system can detect activities at different distances, through a wall, and with multiple people described in section 3 and section 4. We envision our system helping not only with prevention of COVID-19, but supporting contact tracing efforts by monitoring peoples activities at home.

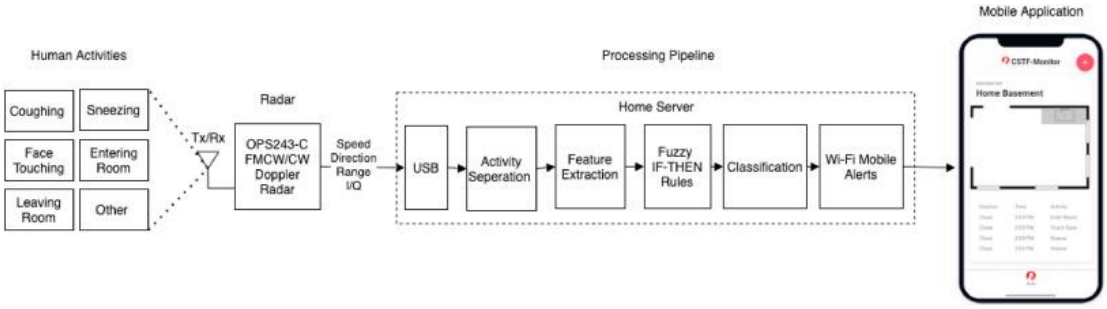

Fig. 1. 15. This figure shows the system architecture from left to right: activities that a human can perform in front of the radar, the radar's transceiver that captures the human activity's motion and outputs the motion's speed, direction, range, and raw in-phase (I) and quadrature-phase (Q) signals, the processing pipeline which consists of a home server that connects to the radar by USB, performs the activity separation, feature extraction, applies the fuzzy IF-THEN rules, classifies the activity, and sends Wi-Fi alerts to a mobile phone, and finally the mobile application which displays the alters from the pipeline including the distance at which the activity was performed, the time the activity was captured, and the type of the activity classified.

The main contributions of our work include the following:

1. We designed a new smart home activity monitoring system that detects coughing sneezing, face touching, and entering/leaving a room with an overall accuracy of 96%. The design includes a mobile application to alert people of the time, location, and type of activity detected. In addition, our system is the first to use a combined CW and FMCW radar for sneeze, cough, and face touching activity detection in the home.

2. We provide solutions for accurately separating activities with a CW and FMCW magnitude filter and differentiating activities with two features and a set of fuzzy logic IF-THEN rules. The features include the interquartile range and relative direction feature of the activity's velocity.
3. We provide an evaluation of our system in different scenarios. We show that with a single individual our system can achieve 96% accuracy. Our systems can detect activities at close, near, and far ranges with 100%, 100%, and 90% accuracy respectively. Our system can detect activities with obstructions such as through a wall with an accuracy of 81%. In addition, our system can detect activities with multiple people with 95% accuracy.

Related Works

There has been a proliferation of research Birring et al. (2008); Sun et al. (2011a, 2015, pp. 97–108); Hata et al. (2009, pp. 1–5); Matos et al. (2006); Monge et al. (2018); Larson et al. (2011, pp. 375–384); Di Perna et al. (2017, pp. 190–193); Amrulloha et al. (2015); Hoyos Barcelo et al. (2018); Pham (2016); Nguyen and Luo (2018); Sun et al. (2011b) focused on the use of audio signals as the primary way of detecting respiratory symptoms such as coughing and sneezing. Devices that include microphones worn as a necklace Birring et al. (2008); Larson et al. (2011, pp. 375–384) have been effective in detecting and counting the frequency of coughs as they are close to the source of the sound. Others have used smartphones Sun et al. (2015, pp. 97–108); Monge et al. (2018) or ubiquitous devices Sun et al. (2011a, pp. 425–434); De Silva (2009, pp. 223–229) and their built-in microphones to detect the sound-related respiratory symptoms. Methods of detection using audio include the

use of fuzzy IF-THEN logic, Hidden Markov Models, or engineered features used to train supervised and semi-supervised models for classification of coughs or sneezes. Most recently Laguarta et al. (2020) developed an AI speech (audio) processing framework that leverages acoustic biomarker feature extractors to pre-screen for COVID-19 from cough recordings using a convolution neural network (CNN). Despite their usefulness, audio sensing systems suffer from environmental noise and obstructions, limited monitoring time due to dependence on batteries, variations in recording conditions such as distance from the microphone, and privacy concerns as many systems continuously monitor audio with a microphone.

Beyond audio sensing other modalities for monitoring respiratory symptoms such as coughing and sneezing include the use of electrocardiogram (ECG), Thermistor, chest belts, Oximeter, and accelerometer, sensors Drugman et al. (2019); Jasmine and Jayanthy (2020). These devices have been effective in detecting voluntary coughs at various volume levels and with background noise, throat clearing, speech and laugh. Recently a new approach Soliński et al. (2020) that uses a portable spirometer device has been developed that can effectively classify the airflow of a cough versus a non-cough. Although promising, most of these devices are required to be always worn by the user, or carried by the user, can be uncomfortable, have limited battery life, and are affected by interference such as rubbing of skin or materials.

In contrast to these past systems, we use RF sensing to detect the motion characteristics of respiratory symptoms related to voluntary coughing and sneezing. The RF sensing technique has more robust properties as RF is not affected by lighting

or environmental sounds, can travel through material, and can report motion information such as speed, direction, and range for an observed activity. For example, Yao et al. (2018, pp. 1718–1726) have shown that RF sensing can be used to detect human motion through walls. Also, privacy can also be preserved, to some extent, when using RF as shown by Li and Zhu (2016a, pp. 571–582). They explain how Doppler signatures are specific to locations of RF antennas in the room and not necessarily associated with an individual. Thus, we used RF to design our system to include: no invasion of personal privacy, by not monitoring conversations with a microphone, monitoring with multiple people in a home, at different distances, through wall detection, and detection without wearing a device or relying on battery power.

Furthermore, our system is not limited to sensing only two activities and can be extended to sense other activities such as face touching and entering/leaving a room. To do this we designed a calibration process described in section 3.5, that allows our system to collect FMCW/CW signatures for any type of activity, which can then be used to define rules to classify the activity performed. These additional, non-respiratory activities, fall under more general activity recognition and have been thoroughly researched Wan et al. (2014); Chi et al. (2016); Li and Zhu (2016b, pp. 238–247); Chi et al. (2018, pp. 237–249); Khan et al. (2016, pp. 1–9); Mahmoud et al. (2020). In this study, we only evaluated a few external motion activities. We did not evaluate our system on internal motion activities such as blood glucose monitoring. Further research could be done to combine our external motion activity detection with smart health devices that do internal health monitoring such as Gao et

al. (2017, 2016, pp. 199–208). Still activities such as touching the face and entering/leaving a room have not been combined with respiratory symptoms such as sneezing and coughing for activity recognition.

About the use of RF sensing for coughs and sneezes, we found very little research. One technique Oncu (2016, pp. 5161–5164) designed a Doppler radar system, that can detect cough and apnea, but only a small experiment was conducted with one observed cough event in a 40 s measurement. Majority of research that uses ambient sensing such as RF or Wi-Fi focus mainly on breathing and heart rate monitoring Nguyen & Tran (2020); Li, Valero, Shahriar, Khan, & Ahamed (2020); Adib et al. (2015, pp. 837–846); Kukkapalli et al. (2016, pp. 1–3); Liu et al. (2015, pp. 267–276). To our knowledge, our system is the first in smart home monitoring of voluntary coughs and sneezes, with the combination of other activities like face touching and entering/leaving a room, using CW/FMCW radar for sensing.

Theory of Operation

Our system uses a combined CW Doppler and FMCW radar to detect motion, speed, direction, and range information from human activities. The basic principle of the radar utilizes the CW Doppler frequency shift to detect the speed and direction or velocity of an activity's motion and the FMCW time of flight (TOF) to detect the range or distance at which activities are performed. This process starts with the radar transmitting a signal. When a person is in the field of view (FoV) of the radar, the transmitted signal will bounce back off the person to the receiver of the radar. The received signal is then mixed with the transmitted signal to down convert to an intermediate frequency signal, representing either the Doppler frequency of the

human motion performed by a person's activity, or a time shift based on the distance to the person performing the activity. We refer the reader to Miller et al. (2019); Wan et al. (2014) and Adib et al. (2013); Solano-Pérez et al. (2020) for a detailed description on how CW Doppler and FMCW radars work. Each activity performed can then be characterized by its motion characteristics, velocity, direction, and distance from the radar. Our systems characterize five types of activities including coughing, sneezing, face touching, and entering and leaving a room shown in Fig. 1. *16*.

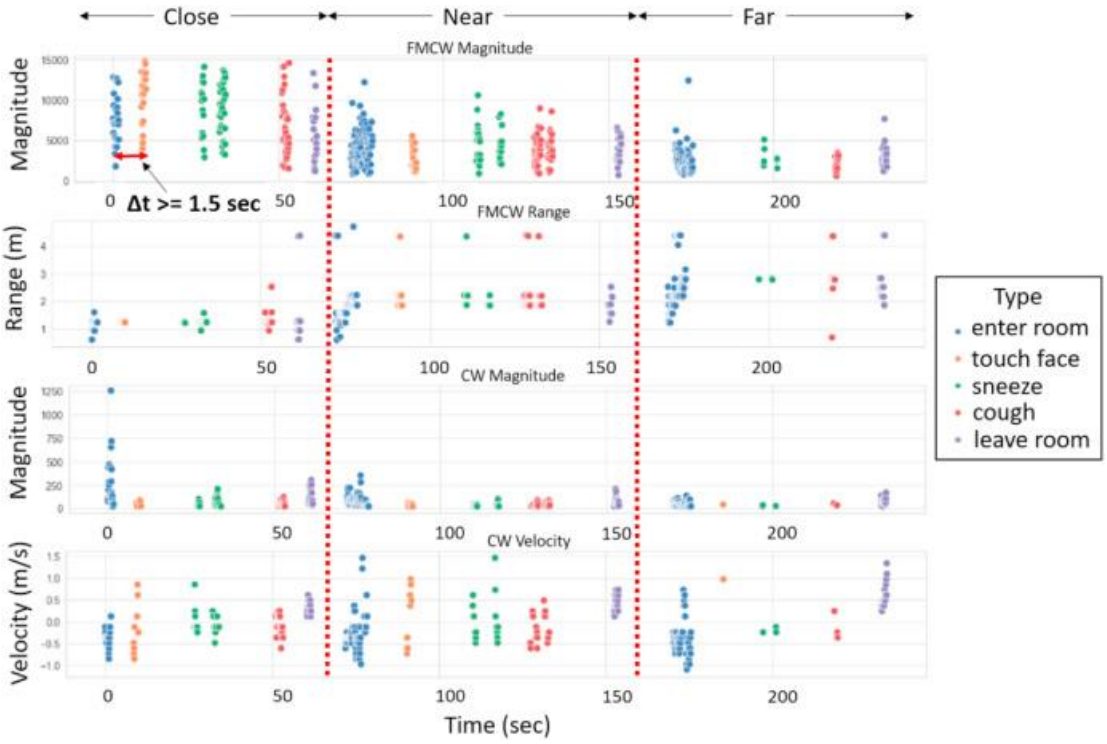

Fig. 1. 16. A total of 19 activities captured over a 4 min continuous period. From top to bottom the figure shows the FMCW magnitude, FMCW range, CW magnitude, and CW velocity. Activities at close range include enter, touch face, sneeze, sneeze, cough and leave. Activities at near range include enter, touch face, sneeze, sneeze, cough, cough, and leave. Activities at far range include enter, touch face, sneeze, sneeze, cough, and leave. Each activity is separated by have a delta t greater than or equal to 1.5 s.

It is important for us to explain the motion events and anatomy phases of each activity we detect. For each activity a different set of phases occurs which produces different reflections back to the radar. These reflections travel further when an object is moving away from the radar and closer when an object is moving towards the radar. We use this principle to show that each activity will have a unique set of reflections which we can use to distinguish them apart from one another. We now explain the motion events and anatomy for each activity: coughing, sneezing, face touching, and enter/leaving a room.

Coughing Anatomy and Motion Events

The anatomy of coughing shown in Fig. 1. *17* is composed of three phases Umayahara et al. (2020): inspiration, compression, and expiration. In the first phase of inspiration, a person inhales air, pressure increases, and there is an expansion of air in the body. During this phase the glottis remains open allowing air in. The glottis is the part of the larynx consisting of the vocal cords and the opening between them. The movement of the chest will be forward or towards the radar as it expands, causing reflections to the radar to be closer or shorter. In addition, we assume that the head moves backward or away from the radar, which causes reflections to the radar to be father or longer. To our knowledge, there is no established or widely agreed upon explanation of the motion of the head in inspiration phase. We assume that inhalation naturally causes the head to move backwards. For the next two phases we also assume certain head motions. In the second phase of compression, the glottis temporarily closes, muscles compress the air in the lungs, and the head is assumed to start to move forward. The compression phase lasts approximately 0.2 s Umayahara

et al. (2020). The increase in pressure causes the reflections from the chest to the radar to be shorter and the head is positioned to move forward and will now be closer to the radar causing the reflection to the radar to be shorter. In the final phase of expiration, the glottis opens resulting in a rapid discharge of the air from the lungs through the mouth. The chest will start to move away from the radar causing the reflection to the radar to be longer and the head is assumed to move forward causing reflection from the head to the radar to be shorter. In general, the radar will receive several reflections, long and short, produced by each phase of coughing. Our system captures these reflections for coughing activities and calculates their FMCW range and magnitude, and CW velocity, and magnitude depicted in Fig. 1. *16*.

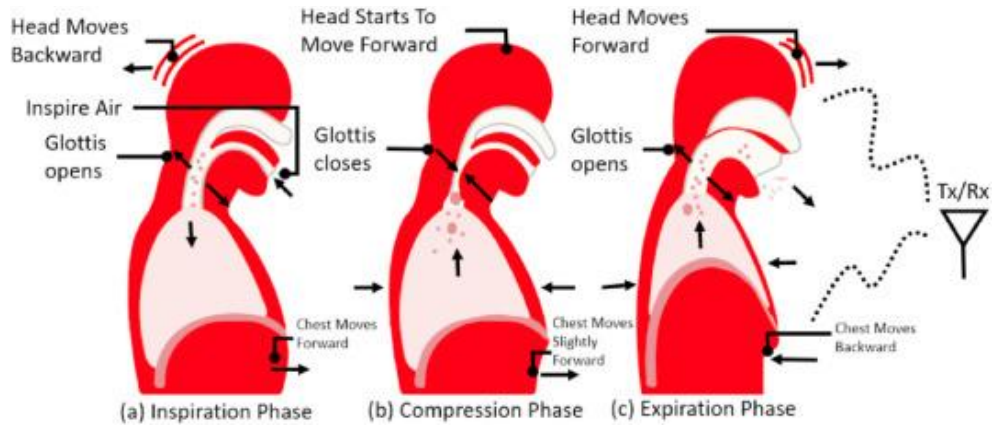

Fig. 1. 17. Anatomy of the cough showing three phases, (inspiration, compression, expiration) and the motions of the chest and head performed during each phase causing short and long radar signal reflections back to the radar.

Sneezing Anatomy and Motion Events

The anatomy of sneezing Songu and Cingi (2009) is shown in Fig. 1. *18* composed of two phases: inspiration and expiration. Typically, inspiration and expiration happen together in a single phase, but we broke them out to show the motion events during each phase. There is usually a phase before inspiration called

the sensitive phase, where there is stimulation of the nasal mucosa by chemical or physical irritants Songu and Cingi (2009). In the inspiration phase of sneezing, a person inhales air, pressure increases, and there is an expansion of air in the body. The movement of the chest will be forward, causing reflection to the radar from the chest to be shorter. We assume that the head moves backwards causing reflection from the head to the radar to be longer. Also, we argue that the glottis does not close all the way, but rather the pallet lowers, and the tongue raises as explained here you (2013). This causes the airway through the mouth to be smaller and the airway through the nose to be larger. This leads to the second phase, expiration where there is a lower increase in pressure since air is compressed less and expands less, during sneeze than cough. The air flow will then be expelled through the nose as the airway is larger when the pallet and tongue are raised. In this phase, the chest will move away from the radar causing reflections from the chest to the radar to be longer. For the motion of the head we assume that it moves forward, and closer to the radar than during coughing. This causes the reflections from the head to the radar to be shorter. From these two phases, the radar will receive several short and long reflections produced by sneezing. Our system captures these reflections for sneezing activities and calculates their, FMCW range and magnitude, and CW velocity and magnitude depicted in Fig. 1. *16*. We assume that sneezing will have more reflections that are shorter over the entire period of both phases. We assumed that when a person sneezes their head will move more forward and at a faster rate towards the radar than a cough. This is one way we can distinguish coughing from sneezing. Although this assumption won't hold for all cases, in our experiments in section 4 which used

voluntary sneezes, we observed the subject moving their head closer to the radar during sneezing than when coughing. Thus, the overall motion of sneezing tends to be more forward or towards the radar than with coughing with a more positive direction as shown in Fig. 1. *24* (b).

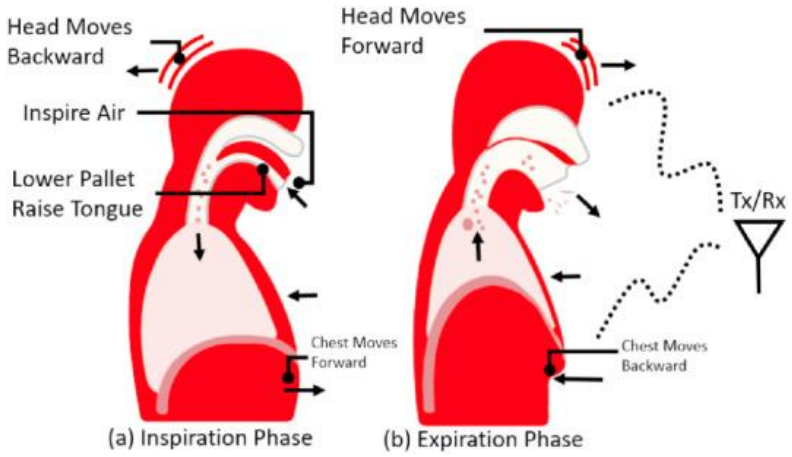

Fig. 1. 18. Anatomy of the sneeze showing two phases, (inspiration and expiration) and the motions of the chest and head performed during each phase causing short and long radar signal reflections back to the radar.

Motion Events for Face Touching

The motion events for face touching, depicted in Fig. 1. *19* (a), can be described in three steps. In the first step we assumed that the person's arm starts at the side of their body naturally hanging down. This leads to the second step, by which the person starts to touch their face by swinging their arm up. The reflections from the arm and hand to the radar will start off shorter as the hand is raised, but over the period that the arm is moving towards the face, majority of the movement will be away from the radar, causing longer reflections back to the radar. In the third step, the person will touch their face and then start to swing their arm down, moving towards the radar causing reflection from the radar to the arm and hand to be shorter. The arm will then go back to its natural position, hanging at the side of their person, and will

move away from the radar casing reflection from the radar to the arm and hand to be longer. Many reflections from the radar during the third step tend to be towards the radar. Our system captures these reflections for each step of face touching and calculates their, FMCW range and magnitude, and CW velocity, and magnitude depicted in Fig. 1. *16*.

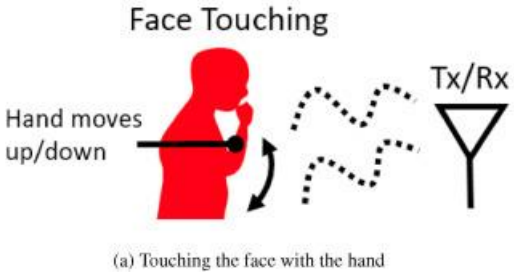

Fig. 1. 19. This figure shows the motion of the arm and hand moving up to touch the face and then back down to the side causing short and long radar signal reflections back to the radar

Motion Events for Entering and Leaving a Room

The motion events for entering and leaving a room, depicted in Fig. 1. *20* (b), are described next. For entering the room, we assumed that the radar was in a position so that when a person entered a room they would be walking away from the radar. The reflections from the radar to the person walking would start of short as the person entered and then get longer as they continued walking away from the radar entering the room. When leaving the room, the reflections from the radar to the person would start off longer, and then get shorter as the person walked towards the radar leaving the room. Our system captures these reflections for entering/leaving a room and calculates their FMCW range and magnitude, and CW velocity, and magnitude depicted in Fig. 1. *16*. Compared to the motions events described previously for coughing, sneezing, and face touching, the direction away and towards for

entering/leaving a room respectively, will be substantially different as shown in 9 (b). We use this knowledge to differentiate the entering/leaving activities from all other activities we captured.

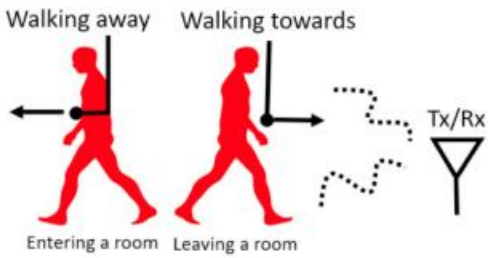

(b) Entering and leaving a room

Fig. 1. 20. This figure shows that when a person is entering a room they are walking away from the radar and when a person is leaving a room they are walking towards the radar causing short and long radar signal reflections back to the radar

System Design

Our system characterizes five types of activities including coughing, sneezing, face touching, and entering and leaving a room with a set of architectural components described next. The architectural components of our system include the OPS243–C FMCW/Doppler radar (OPS243-C 2020) for sensing an activity's motion, a home server that processes, classifies, and produces mobile alerts, and a mobile application that allows the user to view the alert-based notifications shown in Fig. 1. *15*. The FMCW/Doppler radar is capable of detecting speed, direction, and range information for objects in its FoV. In addition, the radar can report the demodulated I/Q signals for calculating the FMCW/CW magnitude. In our setup, we connected the radar via USB to a Raspberry Pi 4 which we used as a home server. The home server acquires radar information for processing. The processing steps include activity separation, calibration, feature extraction, defining a set of fuzzy IF-THEN rules, classification, and the propagation of mobile alerts via Wi-Fi to a mobile application. None of the

processed data is saved on the home server, but is saved on the mobile device storage for historical use. The mobile application, which we named CSTF-Monitor, for cough, sneeze, touch face monitor, can run on both iOS and Android, and allows the user to add a room where the sensor is located and view a table which shows the distance, time, and type of activity detected. The environmental setup used to test our system and processing steps to classify each activity are described next.

Experimental Environment

The environment for our data collection experiments was done in a house in the basement shown in Fig. 1. *21*. The radar was placed 1 m above the ground on a stand. The only furniture in the environment was an office chair, for the subject to sit on. We marked three distances from the radar sensor with tape at 0.91 m, 1.83 m, and 2.74 m for close, near, and far locations. Following our approved institutional review board (IRB) protocol and CDC guidelines for CDC (2020), we made sure to sanitize the area before and after each data collection experiment. Participants were also asked to maintain 6 feet of distance separation from others, as well as wash their hands, use hand sanitizer regularly, and wear a face mask to not spread germs.

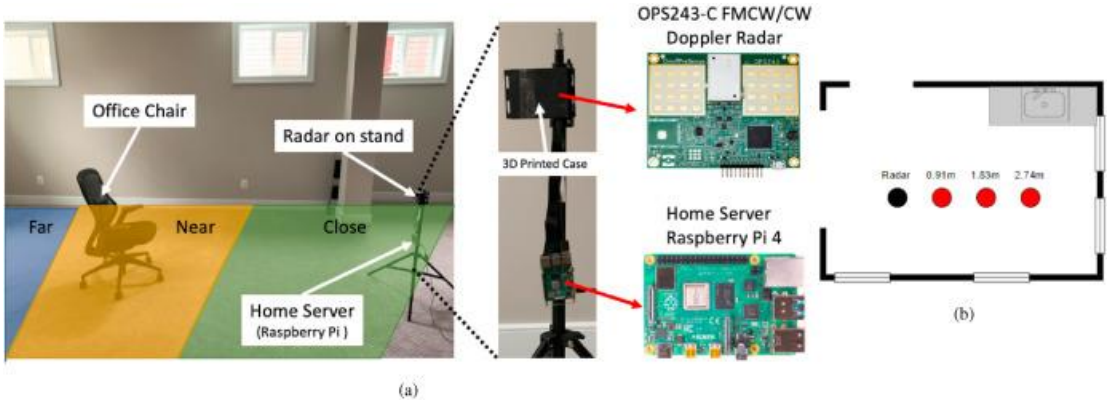

Fig. 1. 21. The environmental setup for data collection experiments including the office chair, the radar and home server attached to a stand, and the locations of far,

close, and near locations (a) and the blueprint layout showing the subject locations depicted as red circles at 0.91 m, 1.83 m, and 2.74 m from the radar (b). (For interpretation of the references to color in this figure legend, the reader is referred to the Web version of this article.)

Capturing and Separating Activities

Our system uses the Doppler velocity magnitude and FMCW range magnitude as a filter to capture each activity separately. To do this we experimentally derived a minimum threshold value M_T of 20 for the Doppler velocity magnitude and FMCW range magnitude. The M_T threshold value is configurable and can be adjusted during calibration. The magnitude for both CW Doppler and FMCW were calculated using the demodulated in-phase I and quadrature-phase Q components of the intermediate frequency signal and calculating the magnitude M at time t as $M(t) = \sqrt{I(t)^2 + Q(t)^2}$. If an activity's magnitude for both the Doppler/FMCW were less than the threshold ($M < M_t$), no measurements are reported, otherwise measurements are reported when ($M > M_t$). Thus, when a subject is still and not moving very much and in front of the radar, the magnitude M will be below the threshold M_T and the radar will not report any data, otherwise if the user moves in front of the radar such that the motion causes the magnitude M to be greater than the threshold M_T then the radar will report motion data. When measurements are reported they include the FMCW magnitude, FMCW range, CW magnitude, and CW velocity shown in Fig. 1. *16.* In order to separate each event from one another, we look for a gap greater Δt than or equal to 1.5 s between each reported value. The Δt gap is configurable and can be adjusted during calibration for activities where Δt happens at a faster or slower interval.

In Home Deployment and Coordination

Our system is capable of being deployed throughout the home to monitor activities in different locations. We did not deploy our system throughout the home, but only deployed it in the basement of the home to conform to our IRB protocol which required a single controlled location for data collection in order to make it easier to follow CDC guidelines for CDC (2020). For deployment throughout a home, at least one of our radar systems would have to be setup in each location that needs monitoring shown in Fig. 1. *22*. Each radar can then be connected by USB to a home server, that contains our processing pipeline shown in Fig. 1. *15*, and a representational state transfer (REST) application programming interface (API) that allows for retrieving alert notifications for each location by hypertext transfer protocol (HTTP) GET methods used by the client mobile application. The home server and mobile application are connected to a wireless home network for communication. For our experiments we used a Raspberry Pi 4 module, which is a credit card sized computer for our home server. To receive alerts, the mobile application client periodically polls the REST API by calling HTTP GET methods for each radar system for alerts. The mobile application can run on both Apple ios and Android platforms and displays an image of the layout of the home, and for each location includes a table that shows the distance (close, near, far) where an activity happened, the time the activity happened, and the type of the activity that happened (sneeze, cough, face touching, entering/leaving a room).

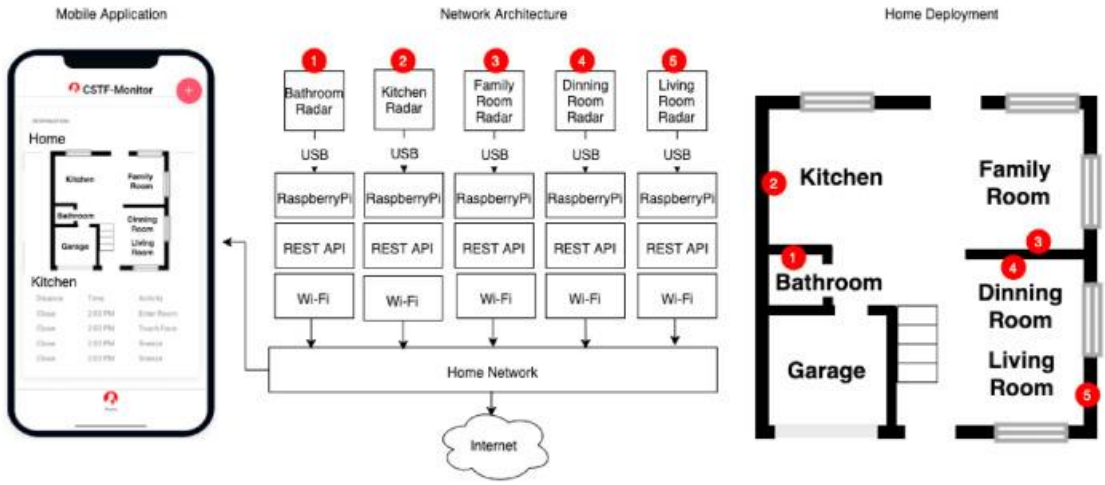

Fig. 1. 22. Home deployment and coordination.

System Calibration Process

Before our system can classify activities, it must be calibrated. The calibration process shown in Fig. 1. *23* is used to capture data related to a specific subject or group of subjects, such as a single family or multiple families. Our calibration process is not limited for data collection related to our specific set of activities (coughing, sneezing, face touching), but can be extended for collecting data related to other activities such as enter/leaving a room which we include in our study. The data captured during the calibration process is used to calculate a set of features which are used to create a set of fuzzy logic IF-THEN rules for accurately classifying activities in the home. The calibration process begins by enabling the calibration mode for the radar. The radar will then apply the magnitude filter we described earlier in section 3.3. Next, the subject will have to walk in front of the radar and sit still. In our setup we wanted to detect activities while sitting, but different positions such as standing could also be done. Then the calibration process will check if there is no motion $M < M_t$, (subject sitting still) for a period t for two cases:

- Case 1: $t > T_1 \; and \; t < T_2$
- Case 2: $t > T_2$

where T_1 is the first-time threshold and T_2 is the second time threshold. When Case 1 for the time of no motion t is true the radar will turn on a LED indicating that the subject can start to perform an activity. While the user is performing an activity the radar will sense and capture motion data if the magnitude $M > M_t$. When the user stops performing the activity the calibration process will then loop back to check for Case 1 or Case 2. When Case 2 is true the subject has either stopped moving for a period $t > T_2$ or has left the FoV of the radar. The radar will then save the captured data for when all Case 2 events were true and turn off the LED to indicate that the calibration processing is done. Lastly the features for creating the fuzzy logic IF-THEN rules will be calculated and the calibration process will stop.

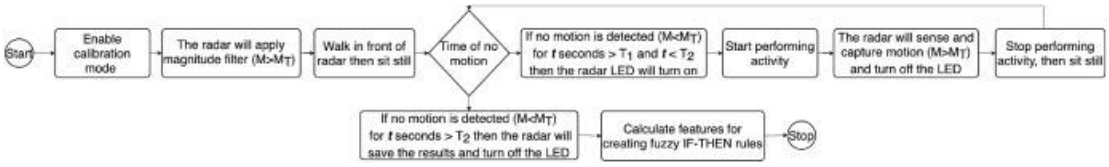

Fig. 1. 23. System calibration process

Initial Calibration for a Single Subject

For initial experiments, for a single subject, we calibrated our system by collecting Doppler and FMCW intermediate frequency signal I/Q, magnitude, range, and velocity information for each activity. Before starting the experiments, we made sure that the subject and principal investigator followed CDC guidelines for CDC (2020), by washing their hands, wearing a face mask, and practicing social distancing of 6 feet from others. The environment was also sanitized before and after a subject was in and out of the room. We used the calibration process described previously in

Fig. 1. *23* for three experiments with a single subject. The subject was asked to perform activities at each distance, 0.91 m, 1.83 m, and 2.74 m, for a total of nine experiments. For each experiment we started by having a subject stand behind the radar, then enter the room. The subject would walk in front of the radar to the labeled location, one of the three distances, and sit still on a chair. When the radar turned the LED on, the subject would perform an activity, and upon completing the activity would sit still again. This was repeated three times pausing for at least 5 s between each activity. Finally, the subject would get up from the chair and walk out of the room by walking towards the radar. We collected three observations for each activity, coughing, sneezing, touching the face, entering/leaving the room, at each of the three distances for a total of 27 observations. For the sneezing activity we asked the subject to perform a voluntary sneeze by taking a deep breath, inhaling air, and mimic a sneeze as described in section 3, by which they would exhale out through their mouth. For the cough activity, we asked the subject to perform a voluntary cough by taking a deep breath, inhaling air, and mimic a cough as described in section 3, by which they would exhale and cough through their mouth at least two or three times. For the other activities the subject was asked to mimic the process as described in section 3. The data collection was done as a manual calibration step, required by our system. We used this set of data to define fuzzy logic IF-THEN rules for activity differentiation described next.

Feature extraction and classification

To differentiate each activity from each other, we calculated two features, the interquartile range (IQR) of the Doppler velocity and the number of positive Doppler

velocity values minus the number of negative velocity values. The IQR describes how spread out the data points for the velocity are from the mean of the velocity for each activity. The positive minus the negative velocity values describes the relative direction of each activity, towards or away from the radar sensor. Using this feature set, we designed two control systems composed of fuzzy logic IF-THEN rules to differentiate and classify each activity. We refer the reader to Bai and Wang (2007, pp. 17–36) for fundamentals on fuzzy logic.

Touching the Face: From our initial data collection experiments we found that the IQR for the activity of touching the face, was the largest amongst all other activities at all distances shown in Fig. 1. *24* (a). We use this knowledge to differentiate touching the face from all other activities using a set of fuzzy logic rules with linguistic variables {‘LOW’,‘HIGH’}. The following fuzzy IF-THEN rules were designed:

- Rule 1: If the IQR of the Doppler velocity is HIGH, THEN the activity measured is touching the face
- Rule 2: If the IQR of the Doppler velocity is LOW, THEN the activity measured is NOT touching the face

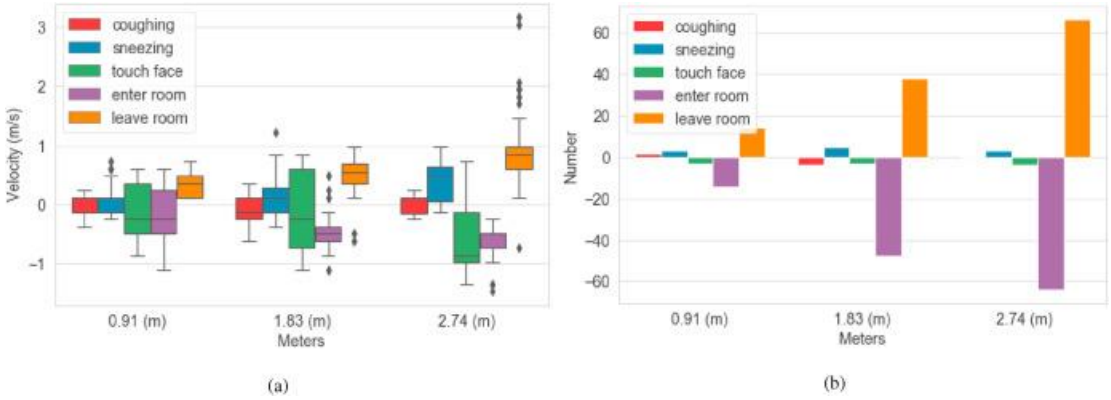

Fig. 1. 24. This figure shows the interquartile range of the Doppler velocity at 0.91 m, 1.83 m, and 2.74 m for each activity (a) and the positive minus negative Doppler velocity feature at 0.91 m, 1.83 m, and 2.74 m for each activity (b).

Entering and Leaving the Room: We also observed that the relative direction for entering the room was low and leaving the room was high when compared to all other activities at all distances shown in Fig. 1. *24* (b). We use this knowledge to differentiate entering/leaving the room from all other activities using a set of fuzzy logic rules with linguistic variables {‘AWAY’,‘STEADY’,‘TOWARDS’} The following fuzzy IF-THEN rules were designed:

- Rule 1: If the direction of the Doppler velocity is AWAY, THEN the activity measured is entering the room
- Rule 2: If the direction of the Doppler velocity is TOWARDS, THEN the activity measured is leaving the room
- Rule 3: If the direction of the Doppler velocity is STEADY, THEN the activity measured is touching the face, coughing, or sneezing

First Fuzzy Control System: We used the designed rules for the activities touching the face and entering/leaving the room to design an aggregate set of rules for our first fuzzy control system. The rules are used to differentiate touching the face from all other activities and leaving/entering the room from all other activities respectively. The activities for coughing and sneezing are grouped into a single membership function and differentiated in a second control system. The universe variables and membership functions for Doppler velocity IQR and the relative direction features as well as the output membership function are shown in Fig. 1. *25*. The parameters were determined experimentally based on the previously collected data for a single subject. For the first control system the following fuzzy IF-THEN rules were designed:

- Rule 1: If the direction of the Doppler velocity is STEADY & the IQR of the Doppler velocity is LOW, THEN the activity measured is sneezing or coughing
- Rule 2: If the direction of the Doppler velocity is STEADY & the IQR of the Doppler velocity is HIGH, THEN the activity measured is touching the face
- Rule 3: If the direction of the Doppler velocity is AWAY, THEN the activity measured is entering the room
- Rule 4: If the direction of the Doppler velocity is TOWARDS, THEN the activity measured is leaving the room

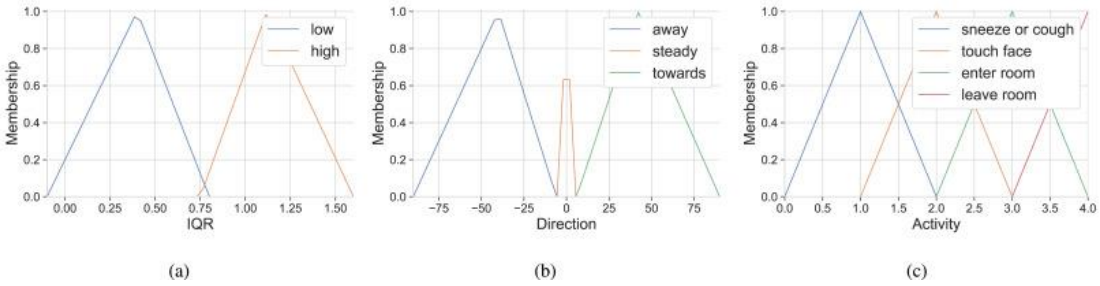

Fig. 1. 25. Control system 1 Doppler velocity IQR membership function (a), Doppler velocity direction membership function (b), and the activity membership function (c).

Second Fuzzy Control System: We used a second fuzzy control system to differentiate between a sneeze and a cough. The second system will be executed only when Rule 1 in the first control system evaluates to true. Then, we redefined the direction membership functions using linguistic variables {'AWAY', 'SOMEWHAT AWAY', 'SOMEWHAT TOWARDS', 'TOWARDS'}. By observing the Doppler velocity relative direction feature shown in Fig. 1. *24*(b), we found that the sneeze and cough can be differentiated by this feature alone. We observed that the sneeze can be somewhat away or towards, while the cough can be somewhat towards and

away. The universe variables and membership functions for the relative direction features as well as the output membership function are shown in Fig. 1. *26*. The parameters were determined experimentally based on the data collected previously. For the second control system the following fuzzy IF-THEN rules were designed:

- Rule 1: IF the direction of the Doppler velocity is SOMEWHAT AWAY OR TOWARDS THEN the activity measured is sneezing
- Rule 2: IF the direction of the Doppler velocity is SOMEWHAT TOWARDS OR AWAY, THEN the activity measured is coughing

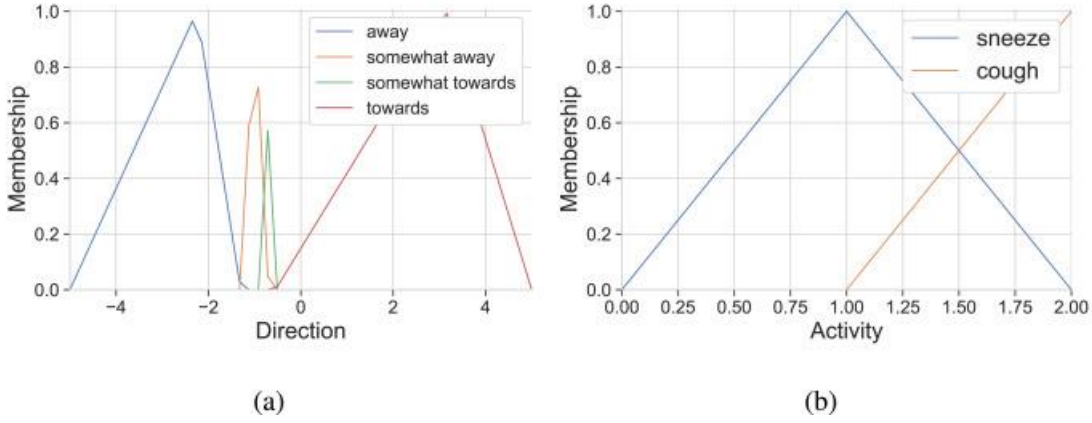

Fig. 1. 26. Control system 2 Doppler velocity direction membership function (a), and the activity membership function (b).

Definition of Distances from the Radar

Our system also detects where an activity happened, either close, near, or far from the radar sensor. The set of distances were defined using fuzzy logic rules with linguistic variables {‘LOW’, ‘MEDIUM’, ‘HIGH’}. To define the fuzzy inputs for the distances we captured human activity range values using FMCW radar at 0.91 m, 1.83 m, and 2.74 m respectively from the radar sensor and observed their root mean square (RMS) distance show in Fig. 1. *27* (a). The output membership function for

the distances is shown in Fig. 1. *27* (b). The following fuzzy IF-THEN rules were designed:

- Rule 1: IF the RMS of FWMC range is LOW, THEN the activity measured was close
- Rule 2: IF the RMS of FWMC range is MEDIUM, THEN the activity measured was near
- Rule 3: IF the RMS of FWMC range is HIGH, THEN the activity measured was far

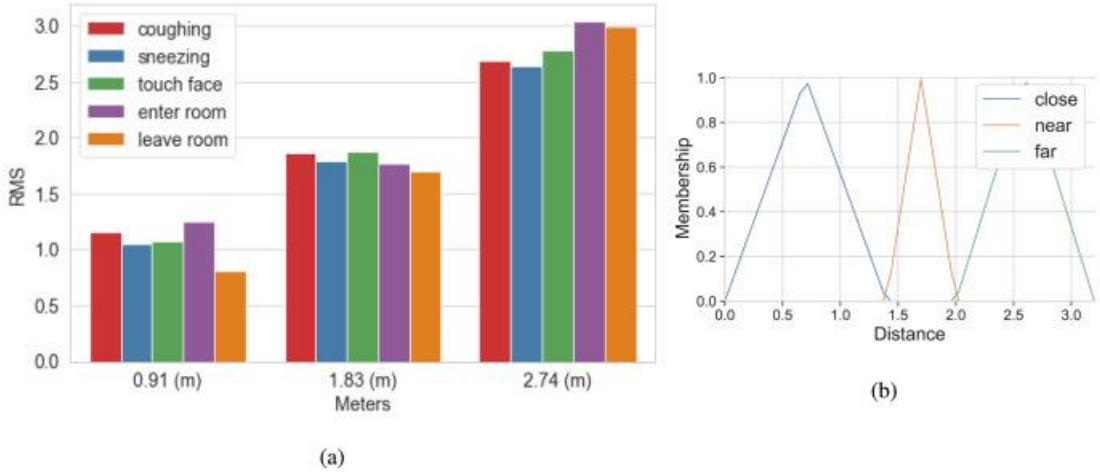

Fig. 1. 27. This figure shows the FMCW RMS range values at 0.91 m, 1,83 m, and 2.74 m. The activities are ordered from left to right: coughing, sneezing, touching face, enter room, and leave room (a) and the FMCW range RMS membership function (b).

Evaluation and Results

We chose to evaluate how well our system can detect a person coughing, sneezing, touching their face, and entering or leaving a room in several different scenarios. The scenarios involved monitoring a single person's activity, monitoring a single person's activities at different distances, monitoring a single person's activities through a wall, and monitoring multiple people's activities. For the first scenario, we

recorded a subject's activity for a total of 4 min shown in Fig. 1. *16*. The subject started behind the sensor then entered the room and sat on a chair. They performed a set of different activities, then left the room. This was repeated three times, at three different distances, for a total of 19 activities observed. We also recorded the subject's activities by observation as a ground truth, which captured a total of 20 activities. One cough activity was not detected at the far distance. As stated before, we followed CDC guidelines for CDC (2020), and had the subject and principal investigator wash their hands, wear a face mask, and practice social distancing of 6 feet from others.

Overall System Accuracy

When running our system for the experiment in Fig. 1. *16*, our system achieved 96% accuracy shown in Fig. 1. 28. There was a single cough activity that was not captured at the far distance. In Fig. 1. *16* there were a total of four cough activities, but our ground truth written observations captured a total of five cough activities. Our fuzzy logic rules and control system were able to detect and classify all 19 observations correctly.

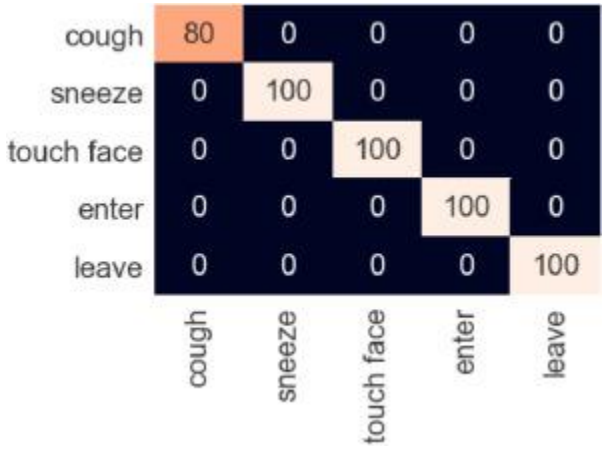

Fig. 1. 28. This figure shows the overall system accuracy for a single subject with a confusion matrix showing the accuracy for each activity detected with total accuracy of 96%. Out of five cough events observed by ground truth video, one cough was not captured

System Accuracy at Different Distances

For each activity in the experiment shown in Fig. 1. *16*, we also applied our fuzzy IF-THEN rules defined for the three distances close, near and far. Our system was able to group each activity accordingly and classify them with 100% accuracy at close distance, 100% accuracy at near distance, and 90% accuracy at far distance shown in Fig. 1. *29*. There were two cough events recorded by written observation at the far distance, but only one was detected.

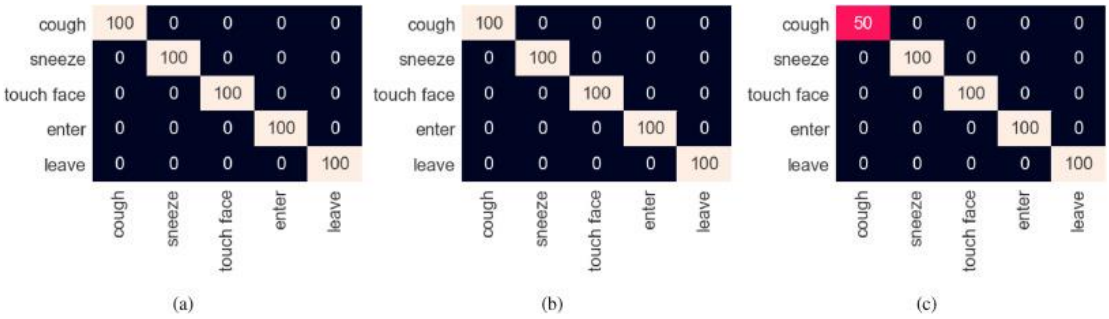

Fig. 1. 29. This figure shows the system accuracy at different distances for a single subject with a confusion matrix showing the accuracy of activities at close with 100% accuracy (a), near with 100% accuracy (b), and far with 90% accuracy. (c) Ranges.

System Accuracy Through a Wall

We also conducted an experiment to test how well our system performs at detecting each activity through a wall. For this experiment, we placed the radar sensor in a bathroom behind a wall. Then we had the subject enter a bedroom adjacent to the bathroom and sit on a chair 1.52 m from the radar shown in Fig. 1. *30* (a). The subject performed a set of activities and then left the room. This was repeated twice for a total of 23 observations. We used the same fuzzy IF-Then rules and membership functions as applied in the experiment in Fig. 1. *16* and achieved an overall accuracy of 81% shown in Fig. 1. *30*(b). We found that our first fuzzy control system grouped all activities with the membership function shown in Fig. 1. *25*(c) with 100%

accuracy. When differentiating the cough and sneeze with our second fuzzy control system using membership function shown in Fig. 1. *26* (b) we achieved only 20% accuracy for detecting a cough and 83% accuracy for detecting a sneeze. The 80% miss-classifications for cough were detected as sneezing and the 16.67% miss-classifications for sneeze were detected as coughing. As mentioned previously, during the experiment, we followed CDC guidelines CDC (2020).

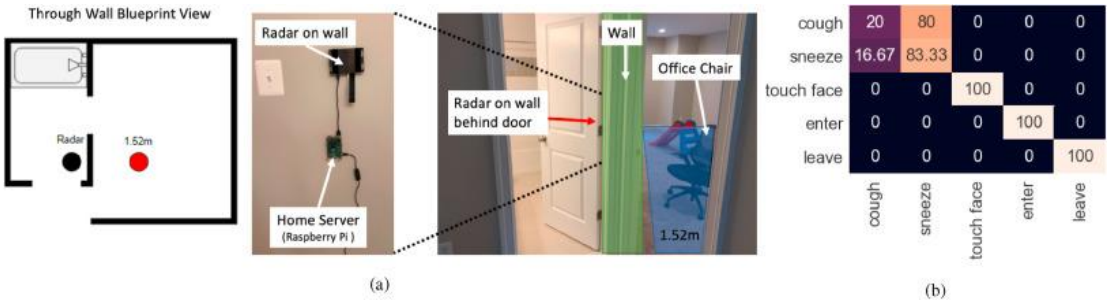

Fig. 1. 30. The environment is set up for detection through a wall. From left to right shows a through wall blueprint showing a black circle for the radar position and the subject location at 1.52 m from the radar depicted by a red circle and the radar shown mounted to a wall in the bathroom behind the door, the wall, and the chair where the subject sat (a), and the confusion matrix showing 81% over all accuracy for activities detected through a wall.

System Accuracy with Multiple People

Lastly, we conducted an experiment to see how well our system performs with multiple people, one male and one female. As mentioned previously, during the experiment, we followed CDC guidelines for CDC (2020) having individuals wash their hands, wear face masks, and practice social distancing. Before conducting the experiment, we had to calibrate our system by collecting data for each person at their respective locations using our calibration process described previously in Fig. 1. *23*. We used the same environmental setup shown in Fig. 1. *21*, but only had one subject sit at 3 ft and the second subject sit at 9 ft from the radar in accordance with our IRB

and CDC protocol for maintaining social distancing of 6 ft. These were the only two locations that we had the subjects sit at. For the initial data collection, we had each subject start behind the radar and then enter the room and sit at one of the two locations. Each subject performed two activities each, taking turns between each activity: touching their face, sneezing, and coughing. Then each subject left the room walking towards the radar one at a time. Using this data set we adjusted the values for each membership function shown in Fig. 1. *31* (a) and (b), and (c). Then we conducted a second experiment where we had each subject stand behind the radar and enter the room one at a time. Each subject sat at the same locations as before, and performed each activity twice, taking turns between each set. Then each subject left the room walking towards the radar one at a time. Between each experiment we made sure to sanitize the area. We recorded a total of 16 activities performed. Then we applied the same fuzzy IF-Then rules defined in our previous control systems and achieved an overall accuracy of 95% shown in Fig. 16 (d). One of the sneezes was miss-classified as a cough.

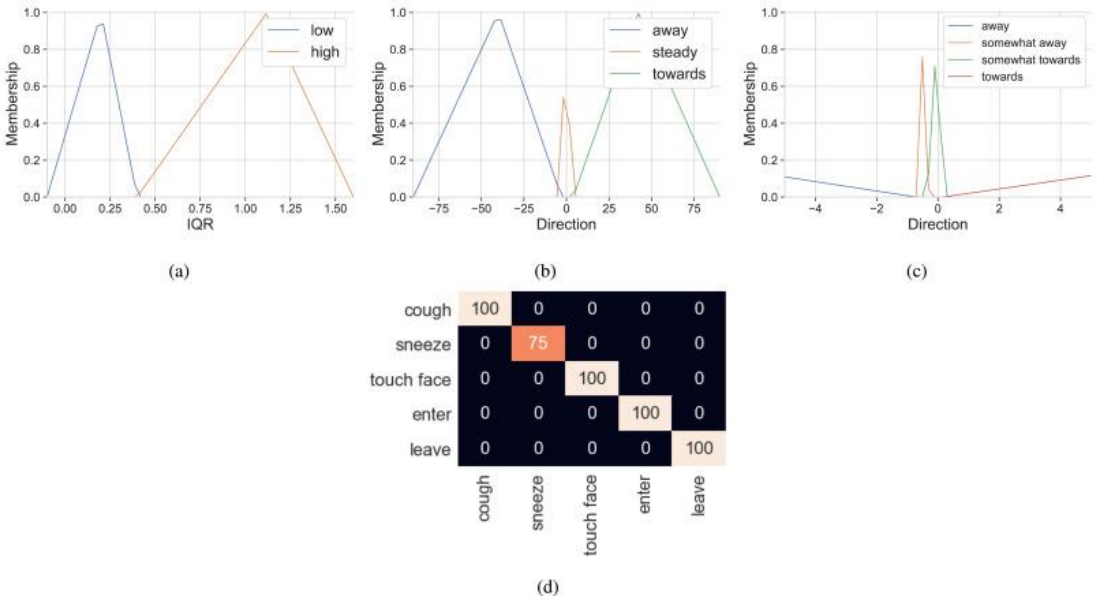

Fig. 1. 31. Multi-person Doppler velocity IQR membership function (a), Doppler velocity direction membership function for control system 1 (b), and the second Doppler velocity direction membership function membership function for control system 2 (c), and the confusion matrix showing the accuracy for each activity detected with multiple people with a total accuracy of 95% (d).

Discussion

Our system is capable of monitoring activities at home including coughing, sneezing, face touching, and entering/leaving room shown in Fig. 1. 28. In addition, we evaluated our system in different scenarios showing that it can detect our set of activities at different distances shown in Fig. 1. *29*, through a wall shown in Fig. 1. *30* (b), and with multiple people shown in Fig. 1. *31* (d). Our system does not require a large historical data set for calibration, but can use a couple examples, three of each activity in our case, to define fuzzy IF-THEN logic rules capable of differentiating each activity from each other. In addition, we identified two features, the IQR, and relative distance feature, to differentiate each activity. The IQR distinctly differentiates face touching from all other activities as observed in Fig. 1. *24* (a). The relative direction feature we created distinctly differentiates enter/leaving a room from all other activities as observed in Fig. 1. *24*(b). We observed that our system can miss-classify a cough for a sneeze or a sneeze for a cough when using the relative direction feature to differentiate the two activities. The relative direction feature does not distinctly differentiate the cough and sneeze from all other activities. In our implementation we expanded the set of linguistic variables for our second fuzzy control system and had to define a new set of fuzzy logic IF-THEN rules to differentiate coughing from sneezing. This is due to the similarity between the motion

movements of the chest and head when sneezing versus coughing. Still our system can accurately detect that a sneeze or cough happened.

Our system also makes some assumptions used to detect and monitor each activity. The first assumption we make is in regard to the placement of the radar. We assume that when our system is used the radar will be positioned in such a way, that when a person enters the room, they will be walking away from the radar. In addition, we assume the radar will be in a position such that when a person leaves the room they will be walking towards the radar. The second assumption we make is that when a person is in a room, and in the FOV of the radar, they are assumed to be quasi-static and sitting on a chair. Quasi-static refers to people sitting still, watching TV, or typing on a laptop. If a person were to get up and starting walking around, then our system would assume the person would be leaving/entering a room, but when a person is sitting our system would assume the person would be performing motions related to coughing, sneezing, and face touching. We also make assumptions about the motion of the head when coughing and sneezing. The motion of the head, during inspiration, compression, and expiration, are assumed to start with the head moving backward and then start to move forward as the person coughs. Similarly we assume the head will move backwards when sneezing during inspiration, and more forwards in relation to a cough, as the person exhales. For arm motion we assume that the person's arm starts at the side of their body, swings up to touch their face, and then after touching their face, swings back down to their side. Lastly, we assume that when multiple people are in the room, they will be separated by some distance, in our case 6 ft for practicing social distancing. There could be cases when multiple people are

sitting next to each other, such as on a couch, but we did not have a chance to test our system for this case as it violated social distancing practices.

Our system has some limitations which we will describe next. The first limitation is that our system must be calibrated for each person at different distances. This is because a set of collaboration data is needed to define the membership functions related to each activity. We argue that this approach works well when there are limited data sets or acquiring a set of training data for a system is unavailable or hard to achieve. In our case, we could not find any existing data sets that have captured motion data from activities related to coughing or sneezing. Also, acquiring data related to coughing and sneezing assumes some health risks, as people collecting the data could get sick from those performing the activities. In our present time, with the onset of COVID-19, acquiring data related to coughing and sneezing is either not an option due to social distancing laws or highly risky. Thus, for our experimentation we performed data in a single-family home with individuals who are healthy and voluntary performed coughing, sneezing, face touching, and entering/leaving activities. We followed our approved IRB protocol and CDC guidelines CDC (2020) to minimize risk during data collection by sanitizing areas before and after each experiment as well as washing hands, wearing face masks, and practicing social distancing. We also limited the number of people in the study to two, as to minimize risk and spread of COVID-19. A second limitation of our system is the detection range and FOV. During our experimentation, we showed that activities could be detected as far as 2.74 m from the radar. The OPS243–C radar that we used in our system is capable of detecting activities at further distances, (50 m–60 m), but we

only evaluated distances based on the room size where our experiments were performed. Further research could be done to experiment and observe how far activities such as coughing, and sneezing could be detected from the radar. The FOV is also limited, but can be increased by adding additional sensors. In regard to activity detection, our system is not limited to the set of activities we defined and can be extended to include others. Although, if additional activities were to be added, then new features may need to be created and a new set of fuzzy logic IF-THEN rules would have to be defined. Our calibration process can be used to collect data related to other activities. Lastly our system is limited to how activities are performed when multiple people are being monitored. If activities from multiple people are happening at the same time at the same distance from the sensor, our system will assume the motion is from one person. This limitation can be avoided by zooming into the FMCW reflections from each individual separately Adib et al. (2015, pp. 837–846). Although, we did not apply this method, our system can still detect activities from multiple people if they perform activities at the same time if they are separated by some distance. Again, we separated each subject by 6 ft to practice social distancing, but further research can be done to see how our system performs when two subjects are closer to each other. Given these limitations, our system is very capable of accurate monitoring, and to our knowledge the first smart home monitoring systems to use CW/FMCW radar to monitor activities including: coughing, sneezing, face touching, and entering/leaving a room. In addition, our mobile application, gives people a more detailed view of the activities performed in their household, allowing them to clean and practice better hygiene.

Chapter 4: Radar-based monitoring system for medication tampering using data augmentation and multivariate time series classification

Summary

Inadvertent use of medication that has been tampered with can cause serious harm. Monitoring how and when medication was last used or touched is important for mitigating risks. In our third healthcare application we present a new radar-based monitoring system that can detect eight different types of tampering methods with three types of medication containers. Our system works by using a FMCW and CW Doppler radar to capture motion speed, direction, and range, which we use for classifying activities. For monitoring activities at home, our system can be set up underneath a kitchen cabinet to monitor medication left out on the countertop. As our system uses radar, we can preserve privacy of individuals as the signatures from the radar are specific to the locations of the antennas and not necessarily associated with an individual. For classifying activities, we created a processing pipeline that extracts a set of features from the raw multivariate time series signals from the radar. We then used three types of data augmentation techniques including jittering, scaling, and magnitude warping, to increase our data sets and increase our classification model accuracy. In addition, we evaluated our system using 5-fold cross validation and with different types of augmentation data sets. Our system can achieve 99% accuracy using a logistic regression classifier with multiple people.

Background

The use of prescription medicine administered at home has risen rapidly. In the most recent 2015–2016 survey by the National Center for Health Statistics (Martin, Hales, Gu, & Ogden, 2019), almost half 45.8% of the U.S. population used prescription drugs. There has also been an increase of 18% usage by children under 12 and an increase of 85% usage in adults over 60. This has led to several problems with at home medication tampering. To clarify, the tampering we refer to is not drug tampering or altering of medicine. Instead, we define tampering as an action related to the packaging that the medication is contained in. For example, we try to answer the question: can I determine if a certain type of medication packaging has been tampered with? To answer this question, one would need to know how and when the medication container was first touched and is the focus of this research. For example, tampering can be done by children who inadvertently misuse medication containers found lying around the house (playing with a pill bottle), or damage medication packaging, or alter the medicine by opening the container. This can lead to unintentional child poisoning which represents an increasingly important global health issue (Jovanov, Talukder, Schwebel, & Evans, 2018). Child safety mechanisms have existed for decades, such as child-resistant bottle caps, saving many lives, but they are not full proof. Some packaging can cause inconvenience and even serious harm or death (Lovegrove et al., 2014). Similarly, adults routinely do not take medication as prescribed, either by non-adherence (DeMeo & Morena, 2014), or by using the wrong dose. Elderly people can also forget to take medication, which is a problem for those with dementia (Moshnyaga, Koyanagi, Hirayama, Takahama, &

Hashimoto, 2016). In other cases, the elderly can accidentally take the wrong medication assuming they have been prescribed several. They could mix medications or grab medication from the wrong place. Additionally, for opiate-dependent patients, it is of most importance to monitor tampering with medication as substance use needs to be regularly observed and tracked (Gutwinski et al., 2013). Storing and monitoring medication containers in a single place can be beneficial for protecting people from misuse. A monitoring system could provide early warnings for patients and care givers when children or others try to access the medication. Thus, there is a need for monitoring medication tampering at home to ensure proper use and safely.

Solutions to the problems discussed previously include smart pill bottles (Aldeer, 2021, Toscos et al., 2020), wearable sensors (Odhiambo, Wright, Corbett, & Valafar, 2021), Radio-Frequency Identification (RFID) tags (McCall, Maynes, Zou, & Zhang, 2010), and human activity tracking using computer vision (Aldeer, Javanmard & Martin, 2018). Most of these solutions focus only on medication adherence and not tampering, but are still applicable. One proposed solution in Kidorf, Brooner, Dunn, and Peirce (2021) describes the use of an electronic pillbox that monitored the tampering of a pillbox lid and the containers. Other solutions using smart pillboxes focus on medication adherence monitoring detecting lid opening, bottle picking and shaking. Computer vision has been used to monitor pill bottle picking, hand over mouth, and drinking a glass of water to name a few. Despite their usefulness, some of these solutions require modification to medication packaging, which can be costly, require to be worn, which can be uncomfortable and have

limited battery life, and rely on good quality video, which may not be ideal in very dark or bright environments.

Dissertation Contributions

To address the limitation of previous systems, we present a new medication tampering monitoring system that uses radar shown in Fig. 1. *32*. Radar has robust properties that allow it to work in environments where computer vision systems fail, such as low/high lighting environments. In addition, our system monitors continuously, does not require a battery, and senses tampering wirelessly for a low-cost solution without any modification to medication packaging. Furthermore, our system preserves privacy as the signals captured by our radar system are specific to the locations of the RF antennas in the room and not associated with individuals. Our system works by using a frequency modulated continuous wave (FMCW) and continuous wave (CW) Doppler radar that can sense speed and range characteristics associated with medication tampering methods. The radar reports a series of multivariate time series signals. Using this information, we built a machine learning pipeline capable of classifying eight different medication tampering methods. We were able to classify a diverse set of activities with 99% accuracy. We did this by using a state-of-the-art multivariate time series classification method known as WEASEL+MUSE and a set of three data augmentation techniques to increase our data set size and limit overfitting during classification. We then validated our solution using 5-fold cross validation. The design, implementation, and evaluation of our system provides the following research contributions:

- A new system for monitoring medication tampering using radar, data augmentation, and multivariate time series classification methods. Our system provides accuracy of 99% and can classify eight tampering methods with three types of medication containers using logistic regression.
- Application of data augmentation using jittering, scaling, and magnitude warping to increase data set size for feature extraction and classification. Using the WEASEL+MUSE feature extraction pipeline, we add data augmentation methods, showing an increased improvement of 25%.
- System evaluation for eight tampering methods including: move bottle lid, shake bottle, move bottle, move pill hand, move pillbox, move pill in box, move pillbox lid, and move pill in blister pack.
- Preliminary evaluation with multiple users. We handle unbalanced data sets and show 99% accuracy across the eight tampering methods with three subjects.

Fig. 1. 32. This figure shows the experimental setup with the radar mounted underneath a kitchen cabinet, the medication below the radar on the counter, and a laptop for monitoring the tampering.

Related Works

Several works have evaluated systems for monitoring medication adherence and are applicable for medication tampering. These systems fit into four categories: smart pill containers, wearable sensors, computer vision, and wireless. Most applications evaluate performance for monitoring different activities associated with medication packaging, such as opening lids, shaking bottles, and picking pills by one hand to name a few. The number of activities that can be monitored is fairly small, usually less than four, and focuses on mainly one type of container (Aldeer, Javanmard et al., 2018). Being able to monitor more activities with different containers is important for building robust systems. In comparison, our system uses radar, a less traditional sensing method, and can classify eight activities with three containers accurately. We present a brief overview of some of these systems, and show how our system address their limitations.

Smart Pill Containers

Smart pill containers such as pill bottles and pillboxes have been modified with different types of sensors for monitoring medication use. In Aldeer, Howard, Martin, and Ortiz (2021) they created a smart bill bottle with accelerometers and a PIP-Tag for low-power wireless transmission of data. In their work they applied an SVM for classification and were able identify up to 16 people who interacted with the pill bottle. However, their system does not detect tampering methods such as opening the lid or shaking the bottle, and only focuses on user identification. Similarly, in

Aldeer, Martin and Howard (2018) they build a pill bottle with accelerometers, a load cell, and a switch cell. With multiple sensors they are able to observe five activities related to pill-intake. Another system in Jovanov et al. (2018) was developed to monitor pill bottle activity using capacitive sensors. Employing a Neural Network, they observed 96.4% accuracy when a child is trying to open a bottle. Still, their system requires several sensors, 15, and is limited as it only focuses on a single tampering method. Commercial electronic pill boxes have also been evaluated in Kidorf et al. (2021). They found that electronic pill boxes are effective in protecting against tampering and help with at home medication management. Lastly, in Lee and Dey (2015) they developed a system called dwellSense for monitoring different activities such as medication/pill taking, phone use, and coffee making. They created an augmented pill box that can detect lid openings and when a pill was taken. Most of the smart pill container systems require modification or additions to pill bottles, which could be costly, and have limited monitoring time due to dependence on batteries. Our system uses radar and does not require any modification or adherence of additional sensors to containers. In addition, our system can detect several more activates, eight, and do so with three types of containers, not just pill bottles.

Wearable Sensors

Wearable sensors for medication adherence have focused mainly on wrist worn watches with accelerometers. In Odhiambo et al. (2021) they used smart watches with accelerometers to detect unscrewing/screwing a pill bottle top, topping the bottle, placing a pill in the mouth, picking up a drink, and setting a drink down. They were able to achieve 97% accuracy using a Neural Network. Their system only

focuses on activities associated with taking medicine from a pill bottle and taking the pill with water and does not include other types of containers. Closely related in Lee and Youm (2021), they used a wrist worn watch with a camera for medication behavior monitoring. In their work they applied a convolutional neural network and were able to get 92.7% accuracy. They identified the usage of cups, hands, bottles, opening of bottles, and taking of pills by the mouth. However, their system captures images with a camera that has to hang below the user's wrist, which can be uncomfortable and can move positions causing incorrect capture of activities. Similarly in Chen, Kehtarnavaz, and Jafari (2014) they use a wrist worn inertial sensor and a Microsoft Kinect for medication adherence, but only recognize two actions of twist cap and hand to mouth. A wrist reminder/tracking system was built in Mondol, Emi, and Stankovic (2016) to remind users to take medicine and track usage. Their system does not focus on medication tampering methods, but does integrate the use of voice commands for usability as wrist warn devices have small screens for interaction. Custom wrist worn medication monitoring systems have been evaluated as will in Lim and Abdullah (2017). They created an accelerometer-based wearable worn on both the right and left wrist for monitoring if people took their medication from a pill bottle to their mouth. In their work they do not show battery usage, which is limited, but do show differences in actions from other activities of daily living. Finally, a non-wrist worn wearable, was evaluated in Kalantarian, Motamed, Alshurafa, and Sarrafzadeh (2016). They created a wearable necklace with a piezo sensor in combination with a smart pill bottle and can detect if pills were consumed or not consumed, swallowing, water sipping, and bottle open/closed. The necklace

can be cumbersome as it has to be worn at all times, and only one type of container was evaluated. In comparison to the wearable systems presented previously, our system does not rely on battery power, uses radar instead of accelerometers, and does not have to be worn. The radar system we built can also detect tampering methods associated with different containers and does not use neural networks which require thousands of labeled data for implementation.

Computer Vision

Computer vision systems have been developed for monitoring medication intake and medication adherence/non-adherence. Most systems utilize cameras and depth sensors for capturing images, with Microsoft Kinect, or just Kinect, being the most popular. In Yamanaka and Moshnyaga (2018) they use the RGB camera and depth sensor on the Kinect to monitor medication intake and non-intake actions, such as hand to mouth and hand to eye, with 94% accuracy. Another Kinect based sensor system in Tucker et al. (2015) monitored variations in a person's gait. They recognized walking orientations such as moving front, back, left and right for medication adherence. Similarly, in Moshnyaga et al. (2016) they used the Kinect with voice commands to guide people through the process of taking medication. In their work they do not report their system accuracy or the failure rate when using voice commands. Other systems have used regular cameras for medication intake monitoring (Ammouri and Bilodeau, 2008, Sohn et al., 2015). However, tracking body parts and medication containers with images alone is difficult, and the use of additional sensing like depth is important for making this task easier. The Kinect and camera-based systems rely on good quality images and extreme brightness, or

darkness can affect their performance. Privacy is a concern as images are captured. Also, obstructions can occur from body parts covering containers or parts of the face like the mouth. In comparison to our system, we use radar which works well in different environments with varying brightness and darkness. In addition, our system does not capture images preserving privacy and can work when covered with a 3D-printed case.

Wireless Sensing

Most closely related to our work are wireless systems that use radar or RFID tags for medication monitoring. In Zhao, Hoti, Wang, Raghu, and Katabi (2021) they developed a wireless FMCW radar system for detecting medication self-administration using inhalers and insulin pens. They used neural networks and achieved an accuracy above 95%. Their system has 12 antennas and is fairly large, but able to detect distance measurements of movement used for detection. In comparison, our system is much smaller, enabling sensing in smaller areas such as underneath a kitchen cabinet. In addition, our system captures the speed of motion and distance, rather than just the distance alone. In our experiments we use the speed and speed magnitude for classifying eight tampering methods, whereas in Zhao et al. (2021) they only classify two activities. Furthermore, we used time series classification and data augmentation methods allowing for lower compute resources and less training data requirements, when compared to their neural network approach. Similarly related, several works (Becker et al., 2009, El Abkari et al., 2021, McCall et al., 2010) have used RFID tags for medication adherence monitoring. These systems work by attaching an RFID tag to medication containers such as pill bottles. Then an

RFID reader can be used to track each container wirelessly. Although promising, the RFID systems require a tag being adhered to each container, which can fall off, and sensing with Ultra-High Frequency for better communication data rates is costly. In comparison, our system does not require tags to be attached to containers or a separate reader for tracking. In addition, our radar system can send multivariate time series speed data sampled at 10,000 Hz.

System Design

We constructed a medication tampering monitoring system with an off the shelf radar sensor and a software processing pipeline. Our system is capable of detecting up to eight different tampering methods for three types of medication packages described in Section 3.5. The system starts by collecting motion data for an activity performed in the field of view of the radar. We chose to use the OPS243-C FMCW and Doppler radar (OPS243-C FMCW and Doppler Radar Sensor, 2021), which is capable of reporting speed and speed magnitude values for the motion captured. The speed data acquired from the radar is a multivariate time series with 4 dimensions. Each dimension represents a speed value corresponding to a moving object. The radar was set to report speed values in centimeters per second. We also configured the radar with a speed magnitude filter, which would make the radar report speed values when the speed magnitude was above a threshold. This helped with segmenting each activity described in Section 4.5. To identify our set of eight medication tampering methods, we constructed a software pipeline to process and classify the multivariate time series shown in Fig. 1. *33*. The first step in our pipeline is to process the data by removing outliers, segmenting the activity, and padding the

multivariate time series in order to create an activity frame. These processing steps are described in detail in Section 4. An activity frame represents the multivariate time series motion data for a single tampering method. Once the activity frame is constructed, it is passed into the WEASEL+MUSE feature extraction pipeline described in Section 4.6. The WEASEL+MUSE pipeline produces a one-dimensional feature vector which is then passed to a logistic regression classifier. The logistic regression classifier is used to make predictions on which of the eight tampering methods was performed. To train our logistic regression classifier we collected a set of training data described in Section 4. This training data was augmented with three different types of data augmentation techniques to increase our example size and diversify our data set described in Section 4.4.

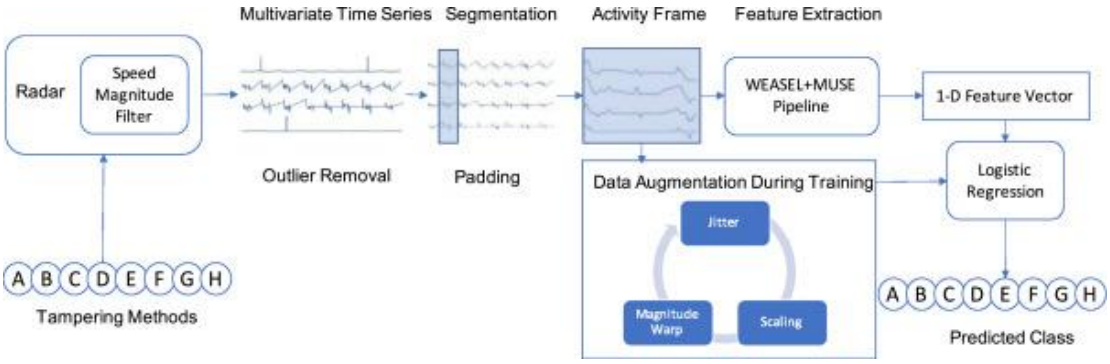

Fig. 1. 33 This figure shows the processing pipeline for identifying the eight tampering methods where: A = Move Bottle Lid, B = Shake Bottle, C = Move Bottle, D = Move Pill Hand, E = Move Pillbox, F = Move Pill in Box, G = Move Pillbox Lid, and H = Move Pill in Blister Pack.

Radar Background

In our system, we use the FMCW and CW Doppler radar to acquire motion information for identifying medication tampering methods. Specifically, we use the 24 GHz OPS243-C radar which can recognize human movement as far as 15 to 20 m. Rather than have two separate radars, one for CW and one for FMWC, the OPS243-C

combines them onto a single platform. Thus, the radar is capable of reporting object speed, direction, and range or distance from the radar at the same time. For detecting speed and direction the radar utilizes the CW Doppler frequency shift and for detecting distance the radar uses the FMCW time of flight (Miller, Banerjee, & Zhu, 2021).

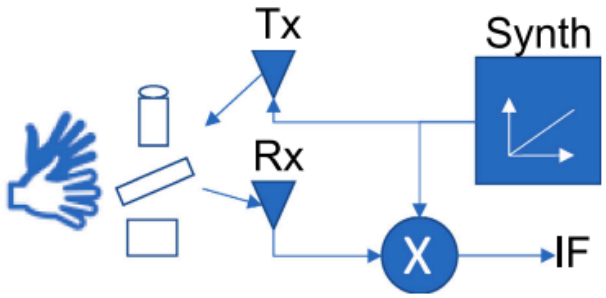

Fig. 1. 34. Simplified block diagram of radar components used to capture IF signal

Sensing with the radar begins with a synthesizer that generates a chirp waveform and transmits the waveform out on a transmitting antenna (Tx). When a person starts to tamper with one of the medication containers, the transmitted waveform is reflected off the hands and the medication container and received at the receive antenna (Rx) of the radar. Once the waveform is acquired the Tx and Rx signals are mixed to obtain the intermediate frequency (IF) signal. We show a simple block diagram of this process in Fig. 1. *34*. This can be described using the following equations (Li, Lei, Yan, Solovey, & Pahlavan, 2020):

$$X_{TX} = \sin[\omega_{TX} \times t + \phi_{TX}]$$

$$X_{RX} = sin[\omega_{RX} \times t + \phi_{RX}]$$

$$X_{OUT} = sin[(\omega_{TX} - \omega_{RX}) \times t + (\phi_{TX} - \phi_{RX})]$$

where X_{TX} and X_{TX} represent the two input sinusoids for the Tx and Rx and the X_{OUT} is the mixed output of the two sinusoids representing the IF signal. Here ω

represents the frequency and ϕ represents the phase. The IF signal is then amplified, low pass filtered, sampled with an analog to digital converter (ADC), and passed to a processing unit. The IF signal will have frequencies corresponding to reflection from multiple objects and can be observed by performing a fast Fourier transform (FFT) on each chirp signal (Wang, Ren, Zhou, Wang, & Yang, 2020). The processing of the FFT takes place on the processing unit. The OPS243-C uses the Cortex M4 ARM processor. When processing the IF signal with the FFT, the frequency of the IF signal will be proportional to the range of the moving hands and medication container. The speed of the hands and medication container are proportional to the Doppler shift. A spectral peak search can be used to obtain the frequencies corresponding to the hands interacting with the medication container. For our purpose, we looked for a total of four spectral peaks, corresponding to four detected objects to obtain multivariate time series information about the speed, direction, and range of the activities performed. We use this information to extract features to train a machine learning classifier to identify the tampering methods discussed in Section 4. All of this processing is configurable and takes place on the radar hardware itself.

Real World Monitoring

Our system can work anywhere around the house to monitor medication containers stored in a single location. To monitor more than one location at a time multiple radars can be set up. For example, a radar could be placed under a kitchen cabinet, inside a bathroom cabinet, inside a dresser drawer, or even from the ceiling to monitor medication containers near a bed, desk, or table. In our experiments we investigate one of these scenarios (medication stored under a kitchen cabinet), but

further experiments can be done to explore different scenarios. Due to the configuration of our radar only having a single patch antenna to receive signals, our system is limited in that it cannot detect an object's location in three dimensions. Our radar would need to know the angle or arrival from the reflected object. Thus, our system can only detect one dimensional data from multiple objects at the same time (distance from the radar). However, 3-dimensional tracking radars exist with multiple Rx antennas to calculate angle of arrival, but have higher cost, require more complex hardware, and use more energy. Thus, to minimize complexity, resources, cost, and use, we chose a FMCW radar that can report distance and speed from the radar, but not the exact position (x,y,z coordinates) from the radar.

Benefits of Using Radar

When monitoring medication, it is advantageous for a system to be covert and not readily noticeable. Such cases arise from not wanting others to damage, remove, or disable the system, so that tapering will go unnoticed. In addition, systems should be robust, being able to work in different environments, such as darkness, and high intensity lighting. In addition, systems should be small, compact, and unobtrusive. Radar addressed these concerns and is a great solution as the primary sensing technology for medication tampering applications. Some benefits of using radar for medication tampering include:

- Privacy: Privacy can also be preserved, to some extent, when using RF as shown by Li and Zhu (2016). When using a radar the Doppler signatures are specific to locations of RF antennas in the room and not necessarily associated with an individual.

- Robustness in environments: Radar can work in complete darkness, in smoky conditions, as well as in high light intensity and low light intensity environments (Patra, Geuer, Munari, & Mähönen, 2018). Thus, medication tampering could be monitored in situations where visibility changes often (near a window), and in constrained or altered environments (kitchen counter, cabinet or drawer).

- Travel through material: Radar signals can also travel through material (Miller et al., 2020) making them a great device for covert operations. For medication monitoring, a radar could be concealed in cabinet, drawer, or ceiling to monitor medication tapering.
- Compactness and distance: Radar systems are also compact, being the size of a credit card or roughly the size of a quarter. They can also sense motion at close and far distances up to 20 or more meters (OPS243-C FMCW and Doppler Radar Sensor, 2021). This is due to the high spatial resolution of radar, and the co-location of transmitters and multiple antennas on a small platform (Patra et al., 2018). This is beneficial for medication tampering monitoring, as systems can be achieved at low cost and work in situations where medication might move to locations at further or shorter distances to the radar.

Types of Medication Containers

Our system can recognize tampering methods for three different types of medication containers shown in Fig. 1. *35*. The containers include a pill bottle, a

pillbox, and a blister pack. The pill bottle has a child resistant lid that requires pushing down and turning to open. The pillbox has 7 compartments for storing medication for each day of the week. Each compartment has a clickable lid that requires pushing up to open and down to close. The blister pack has small clear plastic bubbles with a paper-backed foil to protect medication until it is dispensed. Dispensing medication requires pushing or popping the pill out.

Container	Image
Pill Bottle	
Pillbox	
Blister Pack	

Fig. 1. 35. Medication containers.

Medication Tampering Methods

In this study, we investigated eight types of medication tampering methods for three types of containers and for one case when a pill is put or taken from a hand shown in Fig. 1. *36*. The three types of containers included a screw cap pill bottle, a Monday through Sunday pillbox, and a blister pack. For the pill bottle, we looked at

several tampering methods that included opening the lid, closing the lid, shaking the bottle, taking the bottle, and putting the bottle back. We grouped opening/closing the bottle lid into a single category and called it move bottle lid. For the taking/putting of the pill bottle from the counter, we grouped that into a single category and called it move bottle. For the pillbox we included several types of tampering methods, taking the pillbox and putting the pillbox back, taking a pill from the pillbox, and putting the pill back in the pillbox, and finally opening the pillbox lid and closing the pillbox lid. We grouped the taking/putting of the pillbox on the counter into a single group called move pillbox. For taking/putting a pill in the pillbox we grouped that into a single category called move pill in pillbox. Lastly, we grouped open/close pillbox lid into a group called move pillbox lid. For the blister pack we investigated two tampering methods that included taking a pill from the blister pack and putting a pill back in the blister pack. We grouped taking/putting of the pill in the blister pack into a group called move pill blister pack. Finally, we included a case where a pill was put and taken out of a hand. The taking/putting of the pill in the hand was grouped into a category called move pill hand. The groups were created as the tampering methods that made them up were very similar. Using these eight categories we can identify tampering methods for three common types of medication packaging.

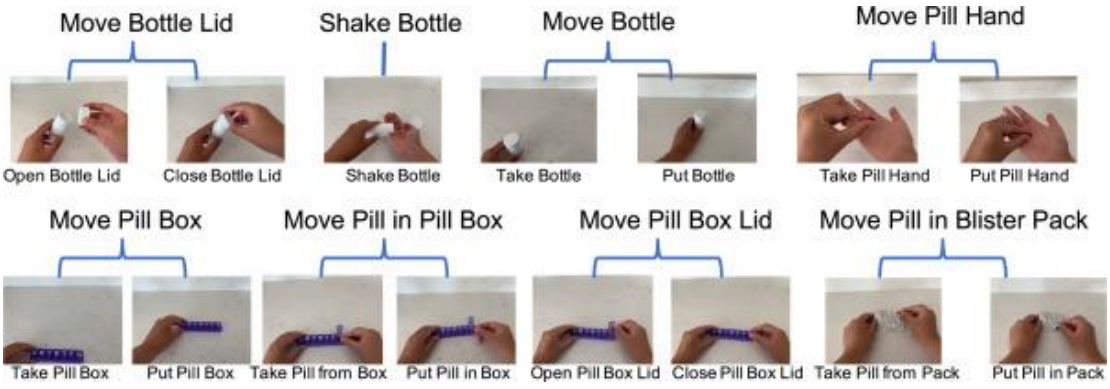

Fig. 1. 36. This figure shows the fifteen medication tampering methods which were grouped together to form eight tampering methods used in our experiments.

Experiments

Typical locations for storing medications include kitchen and bathroom cabinets, or dresser drawers. Location is important as to protect others, small children for example, from tampering with medications. However, there are cases when people forget to put their medication back and leave it out for long periods of time without any monitoring. During the absence of observance is when medication tampering could occur. For this case, we setup our experiments to monitor three types of medication packaging when left on a kitchen counter shown in Fig. 1. *32*. The medication packaging that we used included a pill bottle, a Monday to Sunday pillbox, and a blister pack. To monitor medication tampering we placed the radar underneath a cabinet directed down towards the countertop. In this position we could capture motion directly related to the movement of any of the three medication packages. In addition, directing the radar down was a benefit as it did not pickup background motion, such as people walking around the kitchen, but focused only on motion related to the medication tampering. The radar was connected to a computer to monitor the tampering activities. If the laptop device is not desired, a wireless version of the radar can be implemented so that only a radar and power source would be needed.

Radar Configuration

For our experiments we used our radar with a set of configurations for recording speed and speed magnitude, and range and range magnitude reports to

generate a multivariate time series for each tampering method. The FMCW component was configured to sample at 320,000 Hz, with a sample size of 512, and a range FFT size of 1024. The CW component was configured with a sample rate of 10,000 Hz, sample size of 512, and an FFT size of 512. Speed and range values were configured to be reported in centimeters per second.

Multivariate Time Series

An example of the raw multivariate time series which can be captured with our radar system is shown in Fig. 1. *37*. There are a total of eight tampering methods captured with 4 dimensions for each time series. Our radar system reports the speed values related to four detected moving objects. It does this by applying an FFT to the IF signal and then performing a spectral peak search for a total of four peaks. The peaks in the frequency spectrum correspond to an object detected and is proportional to the distance from the object to the radar. Each speed in the multivariate time series signal is reported in centimeters per second. The speed can be negative or positive in relation to the hands or containers moving away and towards the radar.

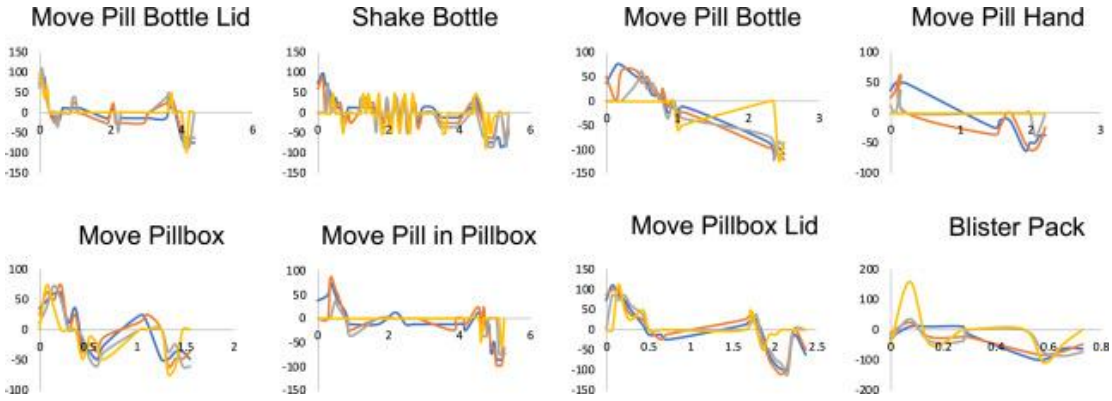

Fig. 1. 37. This figure shows the raw multivariate time series data for eight different tampering methods. Each multivariate time series has four dimensions corresponding to speed in centimeters per second. The speed is on the y-axis and the x-axis represents time in seconds.

Data Collection and Preparation

Collecting data to train a machine learning classifier can be time consuming and difficult to prepare. Challenges arise from ensuring a relatively large sample size and segmenting recorded events, which must be labeled and verified. We will discuss some of these challenges and how we mitigated them to collect quality data. Initially, we collected data for each of the eight medication tampering methods: move lid, shake bottle, move bottle, move pill, move pillbox, move pill in box, move pillbox lid, and move pill in blister pack. The data was collected using the OPS243-C FMCW and Doppler radar sensor. For each medication tampering method performed, a multivariate time series was acquired from the radar. Each multivariate time series had a total of four channels, where each channel represented the speed of motion of four objects in the field of view of the radar. We were able to obtain a total of 296 multivariate time series samples. Once we collected all the data, we took a series of steps to prepare our data for classification as follows:

- **Outlier removal**: We noticed that there were a few data points where the speed values were significantly large, into the thousands, and removed them by replacing them with a zero.
- **Equal lengths**: We also had to make all the multivariate time series the same length by padding the shorter ones with zeros.
- **Balance classes**: We also balanced the classes for each medication tampering method, so that each class had the same number of examples. We did this by truncating a larger set to match the set with the smallest length.

- **Shuffle**: To avoid using the same sample for training and testing our model, we performed a random shuffle of the data.

Small Data Sets and Data Augmentation

Small data sets are a common problem when building original machine learning models (Elton et al., 2018, Um et al., 2017, Zhang and Ling, 2018). The problem lies in not just collecting good data, but also in labeling the data. Collecting and labeling data can be complex and time consuming leading to a limited number of samples collected. In our experiments we collected a total of 296 samples for all the medication tampering methods. Each sample is a multivariate time series with four channels each. The size of our data set would be considered negligible and impractical for advanced machine learning methods like neural networks which require thousands of samples per class. In addition, our data set would be minute for traditional machine learning techniques as it would not allow models to generalize well and cause overfitting. Furthermore, model performance would be poor. Solutions for increasing the size and quality of our data set could include collecting more data or using preexisting data sets that could be combined with our data set. To the best of our knowledge, we could not find preexisting motion data like ours collected with a radar. The majority of available data sets are composed of images, used to train neural networks, and fewer data sets exist for time series.

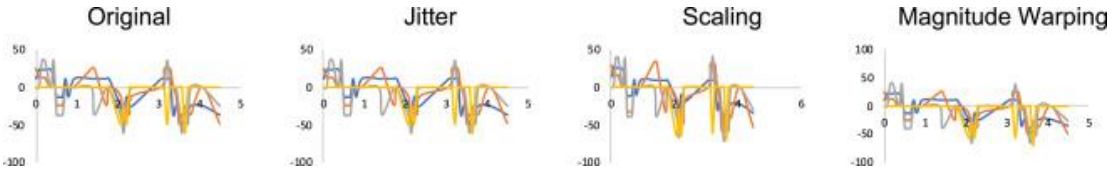

Fig. 1. 38. This figure shows an example of the data augmentation methods used on the original multivariate time series for moving the pill bottle lid. The methods

include jitter, scaling, and magnitude warping. The speed (cm/s) is on the y-axis and the x-axis represents time in seconds.

A less used solution for time series data would be to augment the data to increase the size and diversify the data set. Data augmentation techniques have been applied successfully in the field of computer vision (Taylor & Nitschke, 2017) and include methods such as cropping, permutation, rotating, flipping, and inverting images. Some of these methods have been translated to work on time series data (Um et al., 2017), but not all data augmentation methods are appropriate. When applying augmentation methods, it is important to consider that time series data has temporal data which might affect the model performance if it changes. We found three time series data augmentation techniques that increased our data set and improved our model performance. The three methods we used included jittering, scaling, and magnitude warping. We followed the implementation given by Iwana and Uchida (2021). For each activity we had 4 time series variables or dimensions making them multivariate. Thus, given a multivariate time series (MST) defined as a vector of k time series variables $X_{1t}, X_{2t}, \dots, X_{kt}$ where k is 4, we applied the following:

- **Jittering**: Add random noise to the MST from a Gaussian distribution $\frac{1}{\sigma\sqrt{2\pi}} e^{\frac{-(x-\mu)^2)}{2\sigma^2}}$ with mean μ = 0 and a standard deviation σ = 0.03, based on Um et al. (2017).
- **Scaling**: Increase or decrease the magnitude of all elements in the by multiplying by a scalar. The scalar is computed from a Gaussian distribution $\frac{1}{\sigma\sqrt{2\pi}} e^{\frac{-(x-\mu)^2)}{2\sigma^2}}$ with mean μ = 1 and a standard deviation σ = 0.1, based on Um et al. (2017).

- **Magnitude Warping**: Alter the magnitude of the by convolving the with a curve created by cubic spline. The convolution is performed by multiplying the with a cubic spline with 4 knots at random magnitudes from a Gaussian distribution $\frac{1}{\sigma\sqrt{2\pi}} e^{\frac{-(x-\mu)^2)}{2\sigma^2}}$ with mean $\mu = 1$ and a standard deviation $\sigma = 0.2$, based on Um et al. (2017).

The data was augmented using the original multivariate time series data starting with jittering. Then the original and augmented data was augmented again with scaling. Finally, this was repeated with magnitude warping (MW). As an example, the effects of each augmentation meted is shown in Fig. 1. *38* for moving the pill bottle lid. This process is slightly different from approaches in Iwana and Uchida (2021) and Um et al. (2017) as we created more samples by augmenting the augmented data. After we generated all the augmented data we combined it with our original 296 sample data set to obtain a new data set of 2368 samples. The increase in our data set for each augmentation method is shown in Table 1. *3*. We then applied the preparation steps described previously in Section 4.3.

Table 1. 3. Increase data size with data augmentation

Data Set	Total Examples	MTS Total (4 Dimensions)
Original	269	1184
Jitter + Original	592	2368
Scaling + Jitter + Original	1184	4736
MW + Scaling + Jitter + Original	2368	9472

Event Segmentation

Given a continuous amount of speed data sampled from the radar at 10,000 Hz for the CW signal, we had to separate and label each event. To do this, we created a speed magnitude filter. The filter set a threshold of 5 for the speed magnitude, thus

motion data was only captured when speed magnitude values were above this threshold. The threshold was found experimentally and can be configured if needed. The filter made the task of segmenting each motion event simple, by creating gaps of time between each event. As a result, we segmented motion events for each class by looking for a gap between events of time greater than 2 s. The speed magnitude filter was a feature of that we configured on the radar. We then compared our segmentation counts to hand recorded counts for verification. This process was necessary so that we could proceed with feature extraction and classification.

Event Segmentation

Building a good classifier for multivariate time series is challenging due to the high dimensionality introduced by the multiple univariate time series that make them up (Baydogan & Runger, 2015). Several approaches can be taken to tackle this classification problem. The most basic approach would be to apply a dimensionality reduction method such as principal component analysis (Wold, Esbensen, & Geladi, 1987). Another approach would be to simply concatenate all the dimensions of the multivariate time series into a single univariate time series and use proven univariate time series classification solutions (Rakthanmanon et al., 2012, Schäfer, 2015). However, these approaches can be domain specific, are not noise robust, and do not always consider the relationship of features between dimension (Schäfer & Leser, 2017). Instead we found a relatively new feature extraction method called WEASEL+MUSE that is domain agnostic, and claims to be among the most accurate classifiers when compared to state of the art (Schäfer & Leser, 2017). The WEASEL+MUSE method builds off the bag-of-patterns model and the WEASEL

(Word ExtrAction for time SEries cLassification) pipeline. In addition, WEASEL+MUSE has outstanding robustness on motion recognition data and is why we chose it to extract a set of features from our medication tampering data set. What is different in our approach is that we also extract features from the augmented data we generated and show that WEASEL+MUSE performs well in this scenario. We use WEASEL+MUSE to build a set of histograms over feature counts which we use to train a logistic regression machine learning model. The parameters we used for WEASEL+MUSE were set to strategy being uniform, word size of 4, and a set of windows between sample lengths starting at 5 and ending at 70. We used a logistic regression classifier for multiple classes using the one-vs-rest scheme. The classifier is implemented using liblinear (Fan, Chang, Hsieh, Wang, & Lin, 2008).

Evaluation and Results

To show the improvements in accuracy across all eight medication tampering methods, we compared the classification results of the original data to the classification results with the augmented data. We did the comparison using k-fold cross-validation after following our steps described previously in Sections 4.3, 4.4, 4.5, 4.6. In the k-fold cross validation method, the data is split into k equal folds, of which k-1 folds are used for training. Then the resulting model is validated on the remaining part of the data, the test set, which is then used to compute the accuracy. For our experiments, we chose to set k to 5 for 5-fold cross validation. Other values of k can be used, but values of 2, 5, and 10 are the most widely used (Goyani & Patel, 2017). The results are displayed in Fig. 1. *39*, Fig. 1. *40* as confusion matrices. The original data of 296 examples without augmentation had a total of 74% accuracy,

while the augmented data with 2368 examples had a total of 99% accuracy. This was about 25% improvement in classification accuracy when using the larger data set with augmentation. In addition, each of the eight medication tampering methods improved their accuracy to above 98%. These results are similar to those achieved with other data sets using WEASEL+MUSE with 8 or more classes (Schäfer & Leser, 2017).

Fig. 1. 39. This figure shows the confusion matrix results using the original data set with a total of 74% accuracy. The labels for the 8 medication tampering methods are as follows: A is Move Bottle Lid, B is Shake Bottle, C is Move Bottle, D is Move Pill Hand, E is Move Pillbox, F is Move Pill in Box, G is Move Pillbox Lid, and H is Move Pill in Blister Pack.

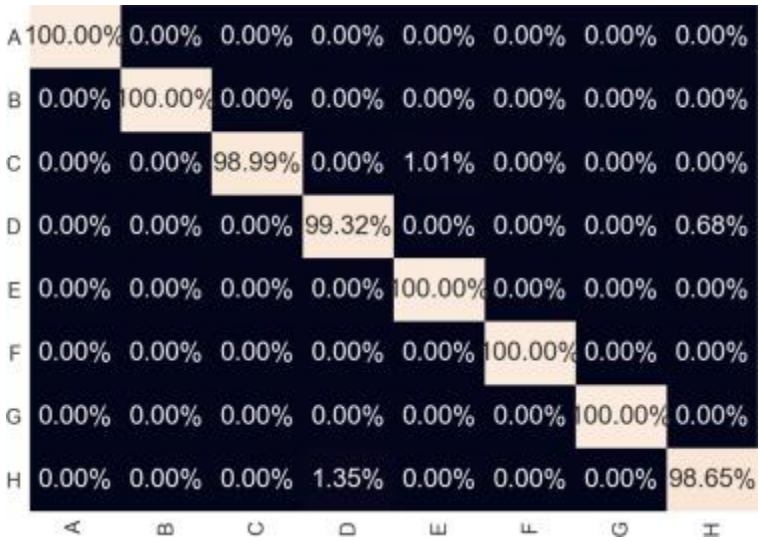

Fig. 1. 40. This figure shows the confusion matrix results using the augmented data set with a total of 99% accuracy. The labels for the 8 medication tampering methods are as follows: A is Move Bottle Lid, B is Shake Bottle, C is Move Bottle, D is Move Pill Hand, E is Move Pillbox, F is Move Pill in Box, G is Move Pillbox Lid, and H is Move Pill in Blister Pack.

Analyzing data augmentation impact on accuracy

We experimented with the impact of data augmentation on our model's accuracy. As mentioned previously in Section 4.4 we used three data augmentation techniques: jittering, scaling, and magnitude warping. For each of these augmentation methods, we assessed their impact on our model's performance as they were added to our original data set one by one. In addition, we experimented with the impact of accuracy as the augmentation data sets were aggregated. For each of these cases we performed 5-fold cross-validation using the same logistic regression classifier. The accuracy results for each experiment is shown in Fig. 1. *41*. As data augmenting takes place you can see that the accuracy increases to above 90% accuracy, with the highest accuracy being the data set with all the augmentation techniques.

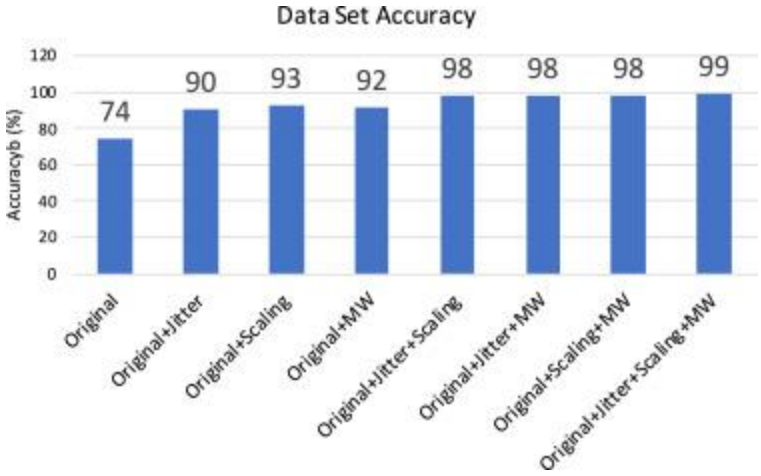

Fig. 1. 41. This figure shows the classification accuracy for different augmentation data sets aggregated with the original data set.

Preliminary experiments with multiple users

We evaluated out system with multiple users. For an initial experiment we collected data from a total of three subjects. Each subject was asked to perform each of the eight tampering methods ten times each. After processing the data we found that the number of examples collected for each of the eight classes was unbalanced amongst the three subjects. In order to evaluate our system performance, we had to balance the classes. To do this we used our data augmentation methods described previously to generate enough classes for the smaller sets. In total, we balanced each class so that they had ten examples for each tampering method for a total of eighty examples for each subject. The initial data counts and balanced data counts are shown in Fig. 1. *42* for comparison. Across the eight tampering methods for the three subjects, we collected 240 examples for our initial data set. Following the same steps described in Section 4.4 we increased our data set using data augmentation to a total of 1920 examples. Then we processed the data through our processing pipeline described in Section 3. Using the same 5-fold cross validation and logistic regression classifier described previously, we were able to achieve 55% accuracy when using the original data without augmentation shown in Fig. 1. *43*. We achieved 99% accuracy when using the original and augmented data set shown in Fig. 1. *44*. Thus, our system achieved an improvement in accuracy of 44%.

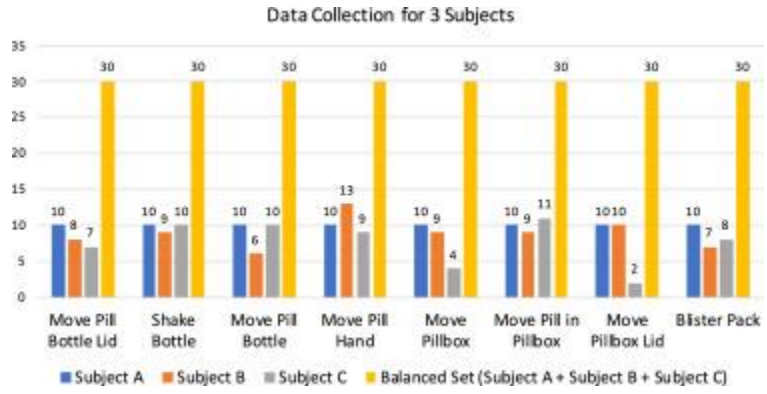

Fig. 1. 42. This figure shows the unbalanced data set collected for three subjects across the eight tampering methods. It also shows the balanced set for each tampering method for comparison.

Fig. 1. 43. This figure shows the confusion matrix results using the original data set for 3 subjects with a total of 55% accuracy. The labels for the 8 medication tampering methods are as follows: A Move Bottle Lid, B Shake Bottle, C Move Bottle, D Move Pill Hand, E Move Pillbox, F Move Pill in Box, G Move Pillbox Lid, and H Move Pill in Blister Pack.

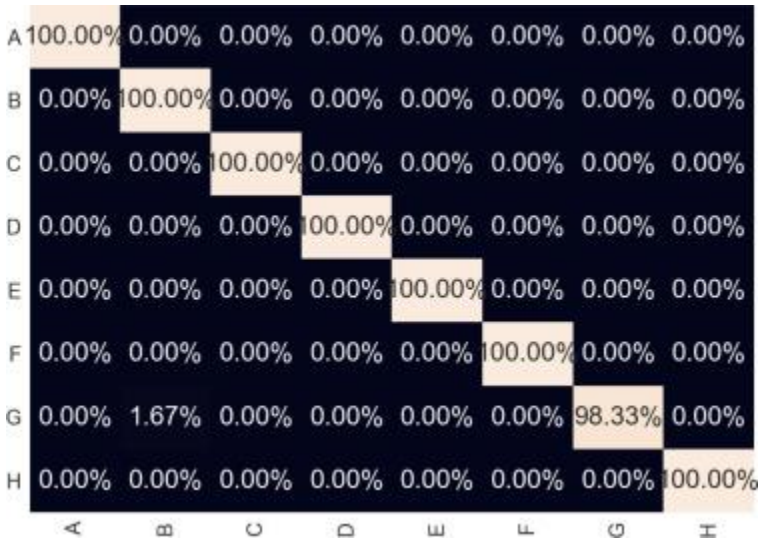

Fig. 1. 44. This figure shows the confusion matrix results using the augmented data set for 3 subjects with a total of 99% accuracy. The labels for the 8 medication tampering methods are as follows: A is Move Bottle Lid, B is Shake Bottle, C is Move Bottle, D is Move Pill Hand, E is Move Pillbox, F is Move Pill in Box, G is Move Pillbox Lid, and H is Move Pill in Blister Pack.

Discussion

We presented a new radar-based monitoring system for medication tampering and pill-taking behaviors capable of detecting eight different types of activities with three types of medication containers. We demonstrated the use of data augmentation methods and WEASEL+MUSE feature extraction to achieve high accuracy for single and multiple users. Moreover, our radar-based system offers multiple benefits compared to other types of medication monitoring systems such as smart pill containers, wearable sensors, computer vision, and wireless RFID systems. Radar has robust properties that allow our system to maintain privacy, operate in dark, smoky, or high light intensity environments, and detect through material such as cabinets while providing a compact and potentially low-cost apparatus to detect medication tampering and adherence. Although we did not demonstrate through material detection, our radar was covered with a 3D printed case when operating and

performed well. Additional experiments could be conducted to see how the system performs when concealed in closed areas such as in a cabinet or drawer.

Further work is needed to test our system with a large number of participants, in different environments, and to differentiate from other motion-behaviors such as eating near a kitchen cabinet or brushing teeth if installed near a bathroom sink. More work is needed to devise a cloud-based and secure transmitting system so that a nearby computer is not needed for the radar-based monitoring system. Also, we envision testing the use of multiple low-cost radars such as the RFbeam Doppler radar K-LC2 with a single unit price: $22.59 (RFBeam 2016) to increase accuracy and the area within which pill-taking motions can be detected, as well as for monitoring medication intake. For example, in Li, Robucci, Banerjee, and Patel (2015) they build a head mounted systems with an array of three K-LC2 radars to detect tongue gestures. This system could potentially be adapted to help with monitoring medication intake.

Another direction to explore would be pairing the system with a smartphone safety notification system to alert users of any unwarranted medication tampering, to keep an automated log of medication adherence, or to alert care providers or family members of missed medication intake. These modalities could be incorporated into pre-existing mobile health (mHealth) interventions such as the Corrie Health platform for self-management in secondary prevention in cardiovascular disease (Spaulding et al., 2019). There is current evidence that mHealth tools can improve adherence among patients with cardiovascular disease (Gandapur et al., 2016) and utilizing the radar-based monitoring system could augment such technology. In addition, a radar-

based monitoring system paired with mHealth technology could be economically efficient and would only require one upfront installment of radars in the user's home, making the entire system more feasible and salable.

The new radar-based monitoring system offers an accurate new tool to detect medication tampering and pill-taking behaviors with unique benefits over other monitoring modalities. Further research is needed to continue the development of this system and possibly combine the system with mHealth technology. In the future, we believe that this new system could present a powerful tool to reduce the dangers of medication tampering by children and to increase medication adherence among a variety of medication users.

Chapter 5: Conclusion

Our dissertation contributions to the field of smart healthcare by showing how useful radar is compared to traditional sensing methods for unexplored use-cases. We showed how radar can preserve privacy, travel through material, work well in challenging environments, is unobtrusive, small, affordable, and compact. These benefits were explored through three smart healthcare applications using radar-based non-contact sensing. Our applications use CW and FMCW radar for sensing and machine learning for thinking and driving intelligent decisions. We show how radar-based non-contact sensing systems can be deployed in the operating room for gesture control and at home to monitor coughing, sneezing, and medication tampering.

In our first smart healthcare application we presented an end-to-end and unobtrusive system that uses Doppler radar sensing to recognize hand and finger gestures when either one hand or both hands are busy. Our system permits the following important capabilities: (1) touch-less input for sterile interaction with connected health applications, (2) hand and finger gesture recognition when either one or both hands are busy holding tools, extending multitasking capabilities for health professionals, and (3) wearable, mobile, and networked, allowing for custom configurations. We evaluated or system in a simulated OR, using five subjects, by training a KNN multi-class classifier achieving 94.5% gesture recognition accuracy. We also tested our real-time system, capable of detecting the start and end of a gesture for classification. We mapped four gestures: double tap, circle, swipe, and finger click to commands to control a CT scan image application. We found that future work is required to evaluate the usability of our system as well as ways to

process the radar signal more accurately in noisy conditions. To the best of our knowledge, this is the first system to successfully use radar for image interaction in the OR.

In our second smart healthcare application we presented a new smart home monitoring system that can detect voluntary coughing, sneezing, face touching, and entering/leaving a room. Our system includes a mobile application with alert notifications for the type, time, and location of the activity detected. To detect, differentiate, and locate each activity, we use a combined CW/FMCW radar to capture the motion speed, direction, and range information. We used two features, the IQR of the velocity, and a relative direction feature, in order to implement a set of fuzzy IF-THEN logic rules which can differentiate activities in different scenarios. We also defined a set of distances, (close, near, far), based on the RMS range values to locate each activity. With a single individual our system can detect activities with an overall accuracy of 96%. In addition, our system can accurately detect activities at different distances (0.91 m, 1.83 m, and 2.74 m), through a wall, and with multiple people. Our system can be used to track activities at home, helping people maintain proper hygiene, knowing which areas to clean and aid in social distancing practices. We envision this system being used to help stop the spread of the devastating COVID-19 virus as well as support contact tracing efforts.

In our third smart healthcare application we presented a new system that uses radar for monitoring medication tampering. Our system is capable of monitoring eight different types of tampering activities using three types of medication containers. We used a pill bottle, pillbox, and a blister pack and detected the following activities:

moving the bottle lid, shaking the bottle, moving the bottle, moving the pill in the hand, moving the pillbox, moving the pillbox lid, and moving the pill in the blister pack. In our setup, we attached the radar underneath a kitchen cabinet to monitor medication containers left on the countertop. In addition, we show how data augmentation methods including jittering, scaling, and magnitude warping can be used to increase our data sets, limit overfitting, and increase our model accuracy. Furthermore, we presented a processing pipeline for multivariate time series classification using the WEASEL+MUSE feature extraction method. Our system achieved 99% accuracy for both single and multiple users evaluated using 5-fold cross validation.

Bibliography

1. Adib, Fadel, et al. "3D tracking via body radio reflections." 11th USENIX Symposium on Networked Systems Design and Implementation (NSDI 14). 2014.
2. Adib, Fadel, et al. "Smart homes that monitor breathing and heart rate." Proceedings of the 33rd annual ACM conference on human factors in computing systems. 2015.
3. Ahmed, Shahzad, et al. "Hand gestures recognition using radar sensors for human-computer-interaction: A review." Remote Sensing 13.3 (2021): 527.
4. Aldeer, Murtadha, et al. "Unobtrusive patient identification using smart pill-bottle systems." Internet of Things 14 (2021): 100389.
5. Aldeer, Murtadha, Mehdi Javanmard, and Richard P. Martin. "A review of medication adherence monitoring technologies." Applied System Innovation 1.2 (2018): 14.
6. Aldeer, Murtadha, Richard P. Martin, and Richard E. Howard. "PillSense: designing a medication adherence monitoring system using pill bottle-mounted wireless sensors." 2018 IEEE International Conference on Communications Workshops (ICC Workshops). IEEE, 2018.
7. Aldeer, Murtadha. "User Identification using Smart Pill Bottles: Systems and Machine Learning Models: PhD Forum Abstract." Proceedings of the 20th International Conference on Information Processing in Sensor Networks (co-located with CPS-IoT Week 2021). 2021.

8. Ammouri, Soufiane, and Guillaume-Alexandre Bilodeau. "Face and hands detection and tracking applied to the monitoring of medication intake." 2008 Canadian Conference on Computer and Robot Vision. IEEE, 2008.
9. Amrulloh, Yusuf A., et al. "Automatic cough segmentation from non-contact sound recordings in pediatric wards." Biomedical Signal Processing and Control 21 (2015): 126-136.
10. Bai, Ying, and Dali Wang. "Fundamentals of fuzzy logic control—fuzzy sets, fuzzy rules and defuzzifications." Advanced fuzzy logic technologies in industrial applications. Springer, London, 2006. 17-36.
11. Barré, René de la, et al. "Touchless interaction-novel chances and challenges." International Conference on Human-Computer Interaction. Springer, Berlin, Heidelberg, 2009.
12. Baydogan, Mustafa Gokce, and George Runger. "Learning a symbolic representation for multivariate time series classification." Data Mining and Knowledge Discovery 29.2 (2015): 400-422.
13. Becker, Eric, et al. "SmartDrawer: RFID-based smart medicine drawer for assistive environments." Proceedings of the 2nd international Conference on Pervasive Technologies Related to Assistive environments. 2009.
14. Birring, S. S., et al. "The Leicester Cough Monitor: preliminary validation of an automated cough detection system in chronic cough." European Respiratory Journal 31.5 (2008): 1013-1018.

15. Bizzotto, Nicola, et al. "Leap motion gesture control with OsiriX in the operating room to control imaging: first experiences during live surgery." Surgical innovation 21.6 (2014): 655-656.
16. Centers for Disease Control and Prevention (CDC)Coronavirus COVID-19 URL:https://www.cdc.gov/coronavirus/2019-nCoV/index.html (2020)
17. Chen, Chen, Nasser Kehtarnavaz, and Roozbeh Jafari. "A medication adherence monitoring system for pill bottles based on a wearable inertial sensor." 2014 36th Annual International Conference of the IEEE Engineering in Medicine and Biology Society. IEEE, 2014.
18. Chi, Zicheng, et al. "EAR: Exploiting uncontrollable ambient RF signals in heterogeneous networks for gesture recognition." Proceedings of the 16th ACM conference on embedded networked sensor systems. 2018.
19. Chi, Zicheng, et al. "Harmony: Exploiting coarse-grained received signal strength from IoT devices for human activity recognition." 2016 IEEE 24th International Conference on Network Protocols (ICNP). IEEE, 2016.
20. Cho, Yongwon, et al. "Enhancement of gesture recognition for contactless interface using a personalized classifier in the operating room." Computer methods and programs in biomedicine 161 (2018): 39-44.
21. De Silva, Liyanage C. "Multi-sensor based human activity detection for smart homes." Proceedings of the 3rd International Universal Communication Symposium. 2009.

22. DeMeo, Dana, and Michael Morena. "Medication adherence using a smart pill bottle." 2014 11th International Conference & Expo on Emerging Technologies for a Smarter World (CEWIT). IEEE, 2014.
23. Di Perna, Leonardo, et al. "An automated and unobtrusive system for cough detection." 2017 IEEE Life Sciences Conference (LSC). IEEE, 2017.
24. Drugman, Thomas, et al. "Objective study of sensor relevance for automatic cough detection." IEEE journal of biomedical and health informatics 17.3 (2013): 699-707.
25. Ebert, Lars C., et al. "You can't touch this: touch-free navigation through radiological images." Surgical innovation 19.3 (2012): 301-307.
26. El Abkari, Safae, et al. "RFID System for Hospital Monitoring and Medication Tracking Using Digital Signature." International Conference on Digital Technologies and Applications. Springer, Cham, 2021.
27. Elton, Daniel C., et al. "Applying machine learning techniques to predict the properties of energetic materials." Scientific reports 8.1 (2018): 1-12.
28. Fan, Rong-En, et al. "LIBLINEAR: A library for large linear classification." the Journal of machine Learning research 9 (2008): 1871-1874.
29. Feng, Yuanyuan, et al. "A virtual pointer to support the adoption of professional vision in laparoscopic training." International journal of computer assisted radiology and surgery 13.9 (2018): 1463-1472.
30. Gallo, Luigi, Alessio Pierluigi Placitelli, and Mario Ciampi. "Controller-free exploration of medical image data: Experiencing the Kinect." 2011 24th

international symposium on computer-based medical systems (CBMS). IEEE, 2011.

31. Gandapur, Yousuf, et al. "The role of mHealth for improving medication adherence in patients with cardiovascular disease: a systematic review." European Heart Journal-Quality of Care and Clinical Outcomes 2.4 (2016): 237-244.
32. Gao, Jialin, et al. "A smart medical system for dynamic closed-loop blood glucose-insulin control." Smart Health 1 (2017): 18-33.
33. Gao, Jialin, et al. "Enhanced wearable medical systems for effective blood glucose control." 2016 IEEE First International Conference on Connected Health: Applications, Systems and Engineering Technologies (CHASE). IEEE, 2016.
34. Gao, Xiaomeng, et al. "Barcode based hand gesture classification using AC coupled quadrature Doppler radar." 2016 IEEE MTT-S International Microwave Symposium (IMS). IEEE, 2016.
35. Goyani, Mahesh M., and Narendra Manorbhai Patel. "Multi-level haar wavelet based facial expression recognition using logistic regression." International Journal of Next-Generation Computing (2018): 131-151.
36. Gu, Changzhan. "Short-range noncontact sensors for healthcare and other emerging applications: A review." Sensors 16.8 (2016): 1169.
37. Gupta, Sidhant, et al. "Soundwave: using the doppler effect to sense gestures." Proceedings of the SIGCHI Conference on Human Factors in Computing Systems. 2012.

38. Gutwinski, Stefan, et al. "Take home maintenance medication in opiate dependence." Deutsches Ärzteblatt International 110.23-24 (2013): 405.
39. Hata, Yutaka, et al. "Human health monitoring system of systems by non-contacted senors." 2009 IEEE International Conference on System of Systems Engineering (SoSE). IEEE, 2009.
40. Hettig, Julian, et al. "Exploration of 3D medical image data for interventional radiology using myoelectric gesture control." Proceedings of the Eurographics Workshop on Visual Computing for Biology and Medicine. 2015.
41. Hoyos-Barceló, Carlos, et al. "Efficient computation of image moments for robust cough detection using smartphones." Computers in biology and medicine 100 (2018): 176-185.
42. Iwana, Brian Kenji, and Seiichi Uchida. "Time series data augmentation for neural networks by time warping with a discriminative teacher." 2020 25th International Conference on Pattern Recognition (ICPR). IEEE, 2021.
43. Jacob, Mithun George, Juan Pablo Wachs, and Rebecca A. Packer. "Hand-gesture-based sterile interface for the operating room using contextual cues for the navigation of radiological images." Journal of the American Medical Informatics Association 20.e1 (2013): e183-e186.
44. Jalaliniya, Shahram, et al. "Touch-less interaction with medical images using hand & foot gestures." Proceedings of the 2013 ACM conference on Pervasive and ubiquitous computing adjunct publication. 2013.

45. Johns Hopkins University (JHU) Covid-19 dashboard by the Center for Systems Science and Engineering URL: https://coronavirus.jhu.edu/map.html (2020)
46. Jovanov, Emil, et al. "Design and feasibility of a safe pill bottle." Applied System Innovation 1.2 (2018): 13.
47. Kalantarian, Haik, et al. "A wearable sensor system for medication adherence prediction." Artificial intelligence in medicine 69 (2016): 43-52.
48. Khan Academy sneeze, cough, and hiccup respiratory system physiology — URL:https://www.youtube.com/watch?v=V2vR5_B6C5I (2013)
49. Khan, Md Abdullah Al Hafiz, et al. "Ram: Radar-based activity monitor." IEEE INFOCOM 2016-The 35th Annual IEEE International Conference on Computer Communications. IEEE, 2016.
50. Kidorf, Michael, et al. "Use of an electronic pillbox to increase number of methadone take-home doses during the COVID-19 pandemic." Journal of Substance Abuse Treatment 126 (2021): 108328.
51. Killick, Rebecca, Paul Fearnhead, and Idris A. Eckley. "Optimal detection of changepoints with a linear computational cost." Journal of the American Statistical Association 107.500 (2012): 1590-1598.
52. Kukkapalli, Ruthvik, et al. "Micro-radar wearable respiration monitor." 2016 IEEE SENSORS. IEEE, 2016.
53. Laguarta, Jordi, Ferran Hueto, and Brian Subirana. "COVID-19 artificial intelligence diagnosis using only cough recordings." IEEE Open Journal of Engineering in Medicine and Biology 1 (2020): 275-281.

54. Larson, Eric C., et al. "Accurate and privacy preserving cough sensing using a low-cost microphone." Proceedings of the 13th international conference on Ubiquitous computing. 2011.
55. Lavielle, Marc. "Using penalized contrasts for the change-point problem." Signal processing 85.8 (2005): 1501-1510.
56. Lee, Hwiwon, and Sekyoung Youm. "Development of a wearable camera and AI algorithm for medication behavior recognition." Sensors 21.11 (2021): 3594.
57. Lee, Matthew L., and Anind K. Dey. "Sensor-based observations of daily living for aging in place." Personal and Ubiquitous Computing 19.1 (2015): 27-43.
58. Li, Fangyu, et al. "Wi-COVID: A COVID-19 symptom detection and patient monitoring framework using WiFi." Smart Health 19 (2021): 100147.
59. Li, Yan, and Ting Zhu. "Gait-based wi-fi signatures for privacy-preserving." Proceedings of the 11th ACM on asia conference on computer and communications security. 2016.
60. Li, Yan, and Ting Zhu. "Using Wi-Fi signals to characterize human gait for identification and activity monitoring." 2016 IEEE First International Conference on Connected Health: Applications, Systems and Engineering Technologies (CHASE). IEEE, 2016.
61. Li, Zheng, et al. "Tongue-n-cheek: non-contact tongue gesture recognition." Proceedings of the 14th International Conference on Information Processing in Sensor Networks. 2015.

62. Li, Ziheng, et al. "ThuMouse: A micro-gesture cursor input through mmWave radar-based interaction." 2020 IEEE International Conference on Consumer Electronics (ICCE). IEEE, 2020.
63. Lim, T. H., and A. H. Abdullah. "Medication Adherence using Non-intrusive Wearable Sensors." EAI Endorsed Transactions on Ambient Systems 4.16 (2017).
64. Liu, Jian, et al. "Tracking vital signs during sleep leveraging off-the-shelf wifi." Proceedings of the 16th ACM international symposium on mobile ad hoc networking and computing. 2015.
65. Lopes, Daniel Simões, et al. "On the utility of 3D hand cursors to explore medical volume datasets with a touchless interface." Journal of biomedical informatics 72 (2017): 140-149.
66. Lovegrove, Maribeth C., et al. "Emergency hospitalizations for unsupervised prescription medication ingestions by young children." Pediatrics 134.4 (2014): e1009-e1016.
67. Lv, Wenjie, et al. "Non-Contact Monitoring of Human Vital Signs Using FMCW Millimeter Wave Radar in the 120 GHz Band." Sensors 21.8 (2021): 2732.
68. Mahmoud, Nourelhoda M., Hassan Fouad, and Ahmed M. Soliman. "Smart healthcare solutions using the internet of medical things for hand gesture recognition system." Complex & intelligent systems 7.3 (2021): 1253-1264.
69. Martin C.B., Hales C.M., Gu Q., Ogden C.L. Prescription drug use in the United States, 2015–2016 cdc.Gov (2019)

70. Matos, Sergio, et al. "Detection of cough signals in continuous audio recordings using hidden Markov models." IEEE Transactions on Biomedical Engineering 53.6 (2006): 1078-1083.
71. McCall, Corey, et al. "RMAIS: RFID-based medication adherence intelligence system." 2010 Annual International Conference of the IEEE Engineering in Medicine and Biology. IEEE, 2010.
72. Mentis, Helena M. "Collocated use of imaging systems in coordinated surgical practice." Proceedings of the ACM on Human-Computer Interaction 1.CSCW (2017): 1-17.
73. Mentis, Helena M., Amine Chellali, and Steven Schwaitzberg. "Learning to see the body: supporting instructional practices in laparoscopic surgical procedures." Proceedings of the SIGCHI conference on human factors in computing systems. 2014.
74. Miller, Elishiah, et al. "RadSense: Enabling one hand and no hands interaction for sterile manipulation of medical images using Doppler radar." Smart Health 15 (2020): 100089.
75. Miller, Elishiah, Nilanjan Banerjee, and Ting Zhu. "Smart homes that detect sneeze, cough, and face touching." Smart Health 19 (2021): 100170.
76. Mondada, Lorenza. "Working with video: how surgeons produce video records of their actions." Visual studies 18.1 (2003): 58-73.
77. Mondol, Abu Sayeed, Ifat Afrin Emi, and John A. Stankovic. "MedRem: An interactive medication reminder and tracking system on wrist devices." 2016 IEEE Wireless Health (WH). IEEE, 2016.

78. Monge-Álvarez, Jesús, et al. "Robust detection of audio-cough events using local hu moments." IEEE journal of biomedical and health informatics 23.1 (2018): 184-196.
79. Moshnyaga, Vasily, et al. "A medication adherence monitoring system for people with dementia." 2016 IEEE International Conference on Systems, Man, and Cybernetics (SMC). IEEE, 2016.
80. Nestorov, Nikola, et al. "Comparing the utility and usability of the Microsoft Kinect and Leap Motion sensor devices in the context of their application for gesture control of biomedical images." European Society of Radiology (2015).
81. Nguyen, Khuong An, and Zhiyuan Luo. "Cover your cough: Detection of respiratory events with confidence using a smartwatch." Conformal and Probabilistic Prediction and Applications. PMLR, 2018.
82. Nguyen, Thi Phuoc Van, and Thanh Tung Tran. "Microwave Doppler Radar Sensing System for Vital Sign Detection: From Evaluated Accuracy Models to the Intelligent System." Proceedings of the 2020 on Intelligent Cross-Data Analysis and Retrieval Workshop. 2020.
83. O'Hara, Kenton, et al. "Interactional order and constructed ways of seeing with touchless imaging systems in surgery." Computer Supported Cooperative Work (CSCW) 23.3 (2014): 299-337.
84. Odhiambo, Chrisogonas, et al. "MedSensor: Medication Adherence Monitoring Using Neural Networks on Smartwatch Accelerometer Sensor Data." arXiv preprint arXiv:2105.08907 (2021).

85. O'Hara, Kenton, et al. "Touchless interaction in surgery." Communications of the ACM 57.1 (2014): 70-77.
86. OPS243-C FMCW and Doppler radar sensor URL:https://omnipresense.com/product/ops243-c-fmcw-and-doppler-radar-sensor (2020)
87. Patra, Avishek, et al. "mm-Wave Radar Based Gesture Recognition: Development and Evaluation of a Low-Power, Low-Complexity System." Proceedings of the 2nd ACM Workshop on Millimeter Wave Networks and Sensing Systems. 2018.
88. Pham, Cuong. "MobiCough: real-time cough detection and monitoring using low-cost mobile devices." Asian Conference on Intelligent Information and Database Systems. Springer, Berlin, Heidelberg, 2016.
89. Rakthanmanon, Thanawin, et al. "Searching and mining trillions of time series subsequences under dynamic time warping." Proceedings of the 18th ACM SIGKDD international conference on Knowledge discovery and data mining. 2012.
90. RFBeam KLC-2 radar URL:http://www.rfbeam.ch/ (2016)
91. Rossol, Nathaniel, et al. "Touchfree medical interfaces." 2014 36th Annual International Conference of the IEEE Engineering in Medicine and Biology Society. IEEE, 2014.
92. Ruppert, Guilherme Cesar Soares, et al. "Touchless gesture user interface for interactive image visualization in urological surgery." World journal of urology 30.5 (2012): 687-691.

93. Schäfer, Patrick, and Ulf Leser. "Multivariate time series classification with WEASEL+ MUSE." arXiv preprint arXiv:1711.11343 (2017).

94. Schäfer, Patrick. "The BOSS is concerned with time series classification in the presence of noise." Data Mining and Knowledge Discovery 29.6 (2015): 1505-1530.

95. Schwarz, Loren Arthur, Ali Bigdelou, and Nassir Navab. "Learning gestures for customizable human-computer interaction in the operating room." International Conference on Medical Image Computing and Computer-Assisted Intervention. Springer, Berlin, Heidelberg, 2011.

96. Sohn, Soo Yeon, et al. "Alarm system for elder patients medication with IoT-enabled pill bottle." 2015 International Conference on Information and Communication Technology Convergence (ICTC). IEEE, 2015.

97. Solano-Pérez, José Antonio, et al. "Comparison of using mm-wave FMCW radar IF signals against frequency-domain VNAs in the application of the multifrequency bifocusing (MFBF) imaging algorithm." AEU-International Journal of Electronics and Communications 117 (2020): 153103.

98. Soliński, Mateusz, Michał Łepek, and Łukasz Kołtowski. "Automatic cough detection based on airflow signals for portable spirometry system." Informatics in medicine unlocked 18 (2020): 100313.

99. Songu, Murat, and Cemal Cingi. "Sneeze reflex: facts and fiction." Therapeutic advances in respiratory disease 3.3 (2009): 131-141.

100. Spaulding, Erin M., et al. "Corrie health digital platform for self-management in secondary prevention after acute myocardial infarction:

Micore rationale and design." Circulation: Cardiovascular Quality and Outcomes 12.5 (2019): e005509.

101. Sun, Xiao, et al. "SymDetector: detecting sound-related respiratory symptoms using smartphones." Proceedings of the 2015 ACM International Joint Conference on Pervasive and Ubiquitous Computing. 2015.

102. Sun, Zheng, et al. "Coughloc: Location-aware indoor acoustic sensing for non-intrusive cough detection." International Workshop on Emerging Mobile Sensing Technologies, Systems, and Applications. Citeseer, 2011.

103. Sun, Zheng, et al. "Pandaa: physical arrangement detection of networked devices through ambient-sound awareness." Proceedings of the 13th international conference on Ubiquitous computing. 2011.

104. Taewoong Um, Terry, et al. "Data Augmentation of Wearable Sensor Data for Parkinson's Disease Monitoring using Convolutional Neural Networks." arXiv e-prints (2017): arXiv-1706.

105. Tan, Justin H., et al. "Informatics in radiology: Developing a touchless user interface for intraoperative image control during interventional radiology procedures." Radiographics 33.2 (2013): E61-E70.

106. Taylor, Luke, and Geoff Nitschke. "Improving deep learning with generic data augmentation." 2018 IEEE Symposium Series on Computational Intelligence (SSCI). IEEE, 2018.

107. Taylor, William, et al. "A Review of the State of the Art in Non-Contact Sensing for COVID-19." Sensors 20.19 (2020): 5665.

108. Tian, Shuo, et al. "Smart healthcare: making medical care more intelligent." Global Health Journal 3.3 (2019): 62-65.

109. Toscos, Tammy, et al. "Medication adherence for atrial fibrillation patients: triangulating measures from a smart pill bottle, e-prescribing software, and patient communication through the electronic health record." JAMIA open 3.2 (2020): 233-242.

110. Tran, Vinh Phuc, Adel Ali Al-Jumaily, and Syed Mohammed Shamsul Islam. "Doppler radar-based non-contact health monitoring for obstructive sleep apnea diagnosis: A comprehensive review." Big Data and Cognitive Computing 3.1 (2019): 3.5.

111. Tucker, Conrad S., et al. "Machine learning classification of medication adherence in patients with movement disorders using non-wearable sensors." Computers in biology and medicine 66 (2015): 120-134.

112. Umayahara, Yasutaka, et al. "Clinical significance of cough peak flow and its non-contact measurement via cough sounds: A narrative review." Applied Sciences 10.8 (2020): 2782.

113. Üncü, Ahmet. "A 24-GHz Doppler sensor system for cardiorespiratory monitoring." IECON 2016-42nd Annual Conference of the IEEE Industrial Electronics Society. IEEE, 2016.

114. Wan, Qian, et al. "Gesture recognition for smart home applications using portable radar sensors." 2014 36th annual international conference of the IEEE engineering in medicine and biology society. IEEE, 2014.

115. Wang, Jingyu, et al. "Noncontact distance and amplitude-independent vibration measurement based on an extended DACM algorithm." IEEE Transactions on Instrumentation and Measurement 63.1 (2013): 145-153.

116. Wang, Yong, et al. "A novel detection and recognition method for continuous hand gesture using fmcw radar." IEEE Access 8 (2020): 167264-167275.

117. Wold, Svante, Kim Esbensen, and Paul Geladi. "Principal component analysis." Chemometrics and intelligent laboratory systems 2.1-3 (1987): 37-52.

118. World Health Organization Coronavirus disease COVID-19 pandemic URL:https://www.who.int/emergencies/diseases/novel-coronavirus-2019 (2020)

119. Yamanaka, Sho, and Vasily Moshnyaga. "New method for medical intake detection by kinect." 2018 IEEE 61st International Midwest Symposium on Circuits and Systems (MWSCAS). IEEE, 2018.

120. Yao, Yao, et al. "Aegis: An interference-negligible RF sensing shield." IEEE INFOCOM 2018-IEEE conference on computer communications. IEEE, 2018.

121. Yusoff, Yusman Azimi, Ahmad Hoirul Basori, and Farhan Mohamed. "Interactive hand and arm gesture control for 2d medical image and 3d volumetric medical visualization." Procedia-Social and Behavioral Sciences 97 (2013): 723-729.

122. Zhang, Ying, and Chen Ling. "A strategy to apply machine learning to small datasets in materials science." Npj Computational Materials 4.1 (2018): 1-8.

123. Zhao, Mingmin, et al. "Assessment of medication self-administration using artificial intelligence." Nature medicine 27.4 (2021): 727-735.